Analytical Biochemistry 529 (2017) 229–244

Contents lists available at ScienceDirect

Analytical Biochemistry

journal homepage: www.elsevier.com/locate/yabio

Progress towards *in vivo* brain ^{13}C-MRS in mice: Metabolic flux analysis in small tissue volumes

Marta Lai [a, *], Rolf Gruetter [a, b, c], Bernard Lanz [a, d]

[a] Laboratory for Functional and Metabolic Imaging (LIFMET), École Polytechnique Fédérale de Lausanne, 1015 Lausanne, Switzerland
[b] Department of Radiology, University of Geneva, 1205 Geneva, Switzerland
[c] Department of Radiology, University of Lausanne, 1015 Lausanne, Switzerland
[d] Sir Peter Mansfield Imaging Centre, School of Physics and Astronomy, University of Nottingham, Nottingham, United Kingdom

ARTICLE INFO

Article history:
Received 13 August 2016
Received in revised form
19 January 2017
Accepted 20 January 2017
Available online 22 January 2017

Keywords:
^{13}C spectroscopy *in vivo*
Mouse brain metabolism
Metabolic modelling
Glucose metabolism

ABSTRACT

The combination of dynamic ^{13}C MRS data under infusion of ^{13}C-labelled substrates and compartmental models of cerebral metabolism enabled *in vivo* measurement of metabolic fluxes with a quantitative and distinct determination of cellular-specific activities. The non-invasive nature and the chemical specificity of the ^{13}C dynamic data obtained in those tracer experiments makes it an attractive approach offering unique insights into cerebral metabolism. Genetically engineered mice present a wealth of disease models particularly interesting for the neuroscience community. Nevertheless, *in vivo* ^{13}C NMR studies of the mouse brain are only recently appearing in the field due to the numerous challenges linked to the small mouse brain volume and the difficulty to follow the mouse physiological parameters within the NMR system during the infusion experiment. This review will present the progresses in the quest for a higher *in vivo* ^{13}C signal-to-noise ratio up to the present state of the art techniques, which made it feasible to assess glucose metabolism in different regions of the mouse brain. We describe how experimental results were integrated into suitable compartmental models and how a deep understanding of cerebral metabolism depends on the reliable detection of ^{13}C in the different molecules and carbon positions.

1. Introduction

Since its first appearance in the field of brain biomedical imaging in the early '90s [1–6], ^{13}C MRS has been facing arduous challenges in enhancing *in vivo* sensitivity and spatial resolution in small localized volumes. All these efforts were motivated by the unique potential and promise of the ^{13}C isotope in exploring metabolism, enabling the measurement of metabolic rates in intact organs *in vivo*. Different approaches in NMR signal measurement have been developed to overcome limitations induced by the inherent low sensitivity of ^{13}C detection, associated with its low natural abundance (1.1%) and gyromagnetic ratio. To meet the need for signal localization in brain MRS, which is essential in order to remove lipid contamination from the scalp and access regional metabolic rates, NMR sequences had to be adapted.

After pioneering *in vivo* ^{13}C MRS detection of brain metabolites in the rabbit under infusion of [1–^{13}C]Glc [7], ^{13}C MRS showed successful results on the human brain. Although most of the early ^{13}C MRS human studies were based on detection of natural abundance signals [1,2,5,6,8], the technique met its wider success with the combined injection of ^{13}C-enriched substrates like glucose and acetate, as single or multiple substrate intravenous administration. These substrates in their different isotopically labelled forms enabled specific insights on compartmentalized cerebral metabolism in the healthy brain and in various brain diseases in human and animal models when combined with ^{13}C metabolic flux analysis (MFA). In ^{13}C-labelling experiments, the fate of the administered substrate into different metabolic pathways can be analysed by taking advantage of a key asset of ^{13}C MRS, namely the distinct chemical shift of the ^{13}C isotope in different molecules and in different carbon positions in the same molecule. Moreover, in highly resolved ^{13}C spectra, the appearance of ^{13}C-^{13}C *J*-coupling allows additional isotopomer analysis, reaching a new frontier in brain ^{13}C MFA. ^{13}C isotopomer analysis was first pioneered in the '80s in studies of perfused heart [9–12] based on single time point

* Corresponding author. EPFL SB IPHYS LIFMET, CH F1 622 (Bâtiment CH), Station 6, CH-1015 Lausanne, Switzerland.
E-mail address: marta.lai@epfl.ch (M. Lai).

http://dx.doi.org/10.1016/j.ab.2017.01.019
0003-2697/

Abbreviations

BBB	Blood-Brain Barrier
FE	Fractional Enrichment
LDH	Lactate Dehydrogenase
MC	Monte Carlo
MFA	Metabolic Flux Analysis
MRI	Magnetic Resonance Imaging
MRS	Magnetic Resonance Spectroscopy
NMR	Nuclear Magnetic Resonance
SNR	Signal-to-Noise Ratio
TCA	Tricarboxylic Acid Cycle
TE	Echo-Time

measurements. The *in vivo* measurement in a same subject of the whole time course of ^{13}C isotopomers appeared only recently in brain metabolic studies, due to the inherently low sensitivity of ^{13}C detection and limited spectral resolution to observe homonuclear coupling. The advent of ultrahigh field systems and improved detection methods enabled this refined analysis [13–16].

The use of animal models combined with brain ^{13}C MRS opens the perspective of a deeper understanding of neurometabolic aspects in a wide range of brain disorders [17]. Within all animal models, mice and rats play a central role in biomedical research. Although *in vivo* ^{13}C MRS is not yet routinely applied in rodents, several studies already demonstrated its feasibility in the rat brain with its associated MFA [18–26] while analogous mouse brain ^{13}C MRS experiments are only recently appearing [27–31], reaching a new standard of sensitivity in ^{13}C detection. This delay is mainly explained by the reduced size of the mouse brain, which affects SNR noticeably and by the small blood volume in the mouse body, which complicates the measurement of the plasma input function by serial blood sampling, a key element of MFA.

This review will examine how major developments in *in vivo* ^{13}C MRS in human and rat brain have been translated to mice at ultrahigh fields. Technical aspects and methodology of a typical *in vivo* experiment will be at first presented, followed by considerations on the impact of magnet field strength, NMR sequences and RF coils on sensitivity. MFA for compartmental modelling will be examined together with the essential ingredients for estimation of metabolic fluxes. Technical advances in spectral and spatial resolution will be described from a historical perspective, starting with the first ^{13}C labelling experiments to the present state-of-the-art techniques in *in vivo* ^{13}C MRS in rodents. At last, most recent results in mice experiments will be presented together with their impact on modelling strategies.

2. *In vivo* ^{13}C MRS in mice: overview of a general experiment

This review will focus on ^{13}C-labelling experiments in rodents with intravenous infusion of a labelled substrate. Mice experiments are generally based on the same kind of setup as for rat experiments, which appeared earlier in the field for practical reasons, both from the physiological and physical points of view. In a rat experiment, animal preparation is already quite challenging, including the arterial/venous cannulations, substrate infusion, monitoring of anaesthesia and physiological parameters, artificial ventilation and recurrent blood sampling during the whole duration of the experiment. Given the reduced anatomical size in mice, surgical interventions are more critical, since blood vessels are smaller and more fragile, which requires additional caution during manipulations. In rats, surgical intervention includes typically a venous catheter for the injection of the labelled substrate and a second one for arterial blood sampling (Fig. 1A). Blood samples are usually employed to measure glycemia as well as other substrates concentration and fractional enrichment (FE) with high resolution NMR or gas chromatography–mass spectrometry: they are typically collected from a long catheter accessible from outside the magnet bore during the ^{13}C-labelling experiment, implying the withdrawal of a relatively large volume of blood before sampling, due to the related dead volume. The blood withdrawn is usually reinjected through the same line at the end of each sampling procedure to minimize losses. Blood volume in mammals is estimated around 6–7% of total body weight [32–34] resulting in less than 2 mL in a mouse of 30 g compared to around 18 mL in a rat of 270 g [35,36]. This allows repetitive blood sampling in rats over a short duration (several hours) as each sample represents about 1% of the total blood volume (typically ~250 μL), as recommended by ethical guidelines [35–37]. Similar constraints applied to mice result in around 10 μL of volume for repeated sampling which is not compatible with experimental needs. Even if the sample would be limited to a significantly small amount sufficient for glycemia measurements, it would even so cause a significant physiological stress due to the rapid decrease in total blood volume during the sampling procedure. Several symptoms would appear among which, a sudden decrease in body temperature and arterial pressure that will ultimately influence cardiac output [38]. If the blood loss reaches 15–20% of the blood volume, compensatory effects would impact the whole body metabolism, including switching to anaerobic glycolysis and acidosis [38], peak rise of blood sugars and fatty acids [39] due to a general hypercatabolism [40]. For these reasons, blood measurements were usually only performed at the end of the experiment for mice in *in vivo* ^{13}C MRS studies [27,28]. Bench experiments performed on a subgroup of similar mice can help to characterize the effect and variability of the infusion protocol and anaesthetics on the blood parameters. Infusion protocols are typically adapted to the specific mouse strain, as well as to the age and sex. In fact each phenotype shows distinct responses to the same protocol caused by specificities in their endocrine systems among others.

For brain ^{13}C-labelling experiments in horizontal MRI magnets, rodents usually lye prone in the magnet bore with an adapted RF coil on the top of their head (Fig. 1A). Anaesthesia can be administered intravenously as frequently done in rats [22,25] but mice protocols more commonly make use of air mixture of volatile anaesthetics, such as isoflurane [27–29,41] with freely breathing animals. Substrates are typically administered through the venous circulation with a catheter placed in a tail or femoral vein. In our group, tail vein lines are connected to a 25G (0.5 mm outer diameter) needle for the injection while a smaller catheter of 26G (0.46 mm outer diameter) is used for femoral vein cannulation The labelled substrate is carried to the brain by the blood circulation, before being taken up through the blood-brain barrier (BBB). Therefore, a precise determination of temporal variation of substrate labelling in plasma, i.e. the arterial input function, is crucial for MFA [42,43]. For this reason, intraperitoneal injections are avoided as they give rise to inconsistent release of the injected substance in plasma. Central to many ^{13}C MRS labelling experiments in the brain is the measurement of mitochondrial oxidative metabolism in the tricarboxylic acid (TCA) cycle as well as further ^{13}C transfer to amino acids, and neurotransmitter cycling. Those biochemical processes are downstream to glucose uptake and metabolism. To achieve optimal characterization of these reactions, an infusion protocol for the entire duration of the experiment is typically designed aiming at reaching a high FE in the blood (on the order of 50–90%) and saturation in the transport through the BBB for the labelled substrate. Transport towards the brain is in fact a

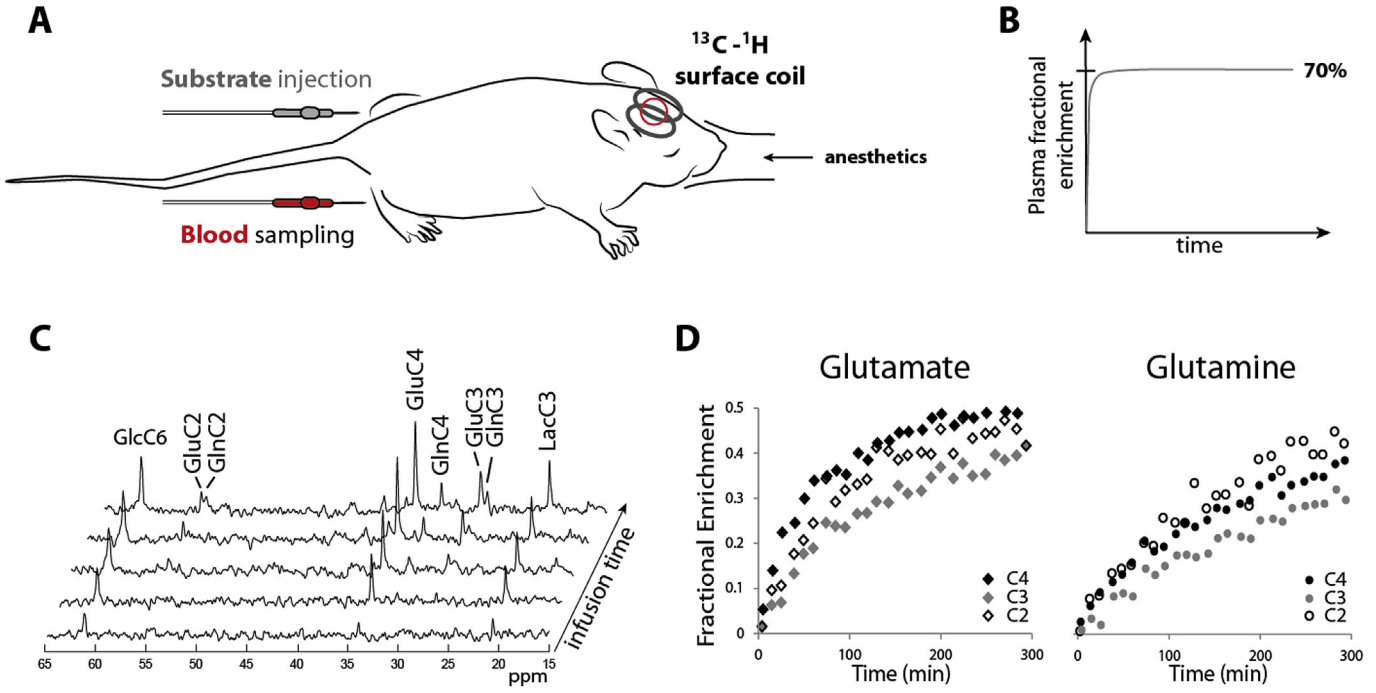

Fig. 1. General setup of a representative *in vivo* ^{13}C MRS experiment in the rat brain (A): the animal is anesthetized with volatile anaesthetics and it lies prone in the magnet with a surface coil on the top of its head. Arterial and venous femoral catheters are put in place in order to access serial blood sampling and allow substrate injection, respectively. The infusion protocol aims to build a step function as plasma input function, by reaching a relatively high level of fractional enrichment for the substrate of choice in the plasma in a short time (<5 min) and maintaining it stable for all the duration of the experiment (B). ^{13}C dynamic spectra show progressively rising peaks of the metabolites carbon positions of glutamate and glutamine and other by-products with sufficiently large pool size (C). Displayed spectra are derived from *in vivo* ^{13}C direct detection in the mouse brain within the first 50 min of infusion of [1,6−^{13}C]glucose at 70% FE. Quantified concentrations of each carbon position from the spectra will constitute the dynamic data set (D) further analysed with MFA to get quantitative information on the metabolic fluxes characterizing the biochemical system under study, typically TCA activity and glutamate/glutamine cycling. Abbreviations: glucose (Glc), glutamate (Glu), glutamine (Gln), lactate (Lac).

mechanism prone to saturation by increasing plasma concentrations as shown for glucose [44], lactate [45] and acetate [46]: this results in a nearly constant extraction rate of the tracer from the blood to the brain compartment, an essential condition to work under metabolic steady state. The ^{13}C-glucose infusion protocol typically consists in a rapid exponentially decaying bolus of 99% enriched glucose, followed by an adjustable continuous infusion of a lower enrichment glucose (typically 60−70%), designed to result in a plasma step function for the labelled precursor fractional enrichment (Fig. 1B). For glucose, an ideal exponential bolus lasts about 5 min where the decaying constant is determined in order to administer almost half of the glucose solution in the first minute. The total bolus volume is calculated based on the animal body weight and the basal glycaemia prior to injection, in order that at the end of the bolus, blood glucose FE reaches the value of the second solution used for the continuous infusion. In this process, the glycemia rises from its basal value (90−110 mg/dL after fasting) to a high value of about 250−300 mg/dL, which also ensures saturation of the transport across the BBB. Such a step input function is of advantage due to its simplicity when aiming at MFA of the

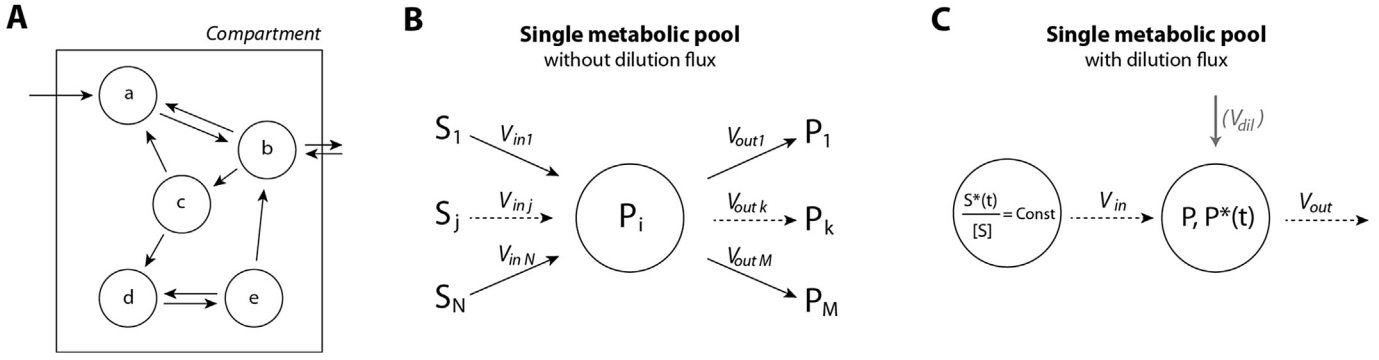

Fig. 2. (A) Representative scheme of a compartment, modelled as an ensemble of single metabolic pools connected by metabolic fluxes. One or several pools can be in direct connection with the external environment. (B) A single metabolic pool scheme with n influxes (V^1_{in}, …, V^n_{in}) coming from n corresponding substrates (S_1, …, S_n). The products (P_1, …, P_m) are generated from the considered metabolic pool through corresponding chemical reactions (V^1_{in}, …, V^m_{in}). (C) Example of a metabolic pool with a single influx (substrate S with a fractional enrichment $\frac{S^*(t)}{[S]}$) and efflux, with the addition of a dilution flux V_{dil} that brings unlabelled isotopes to the product P, reducing the fractional enrichment at steady state $\left(\frac{P^*}{[P]}\right)$.

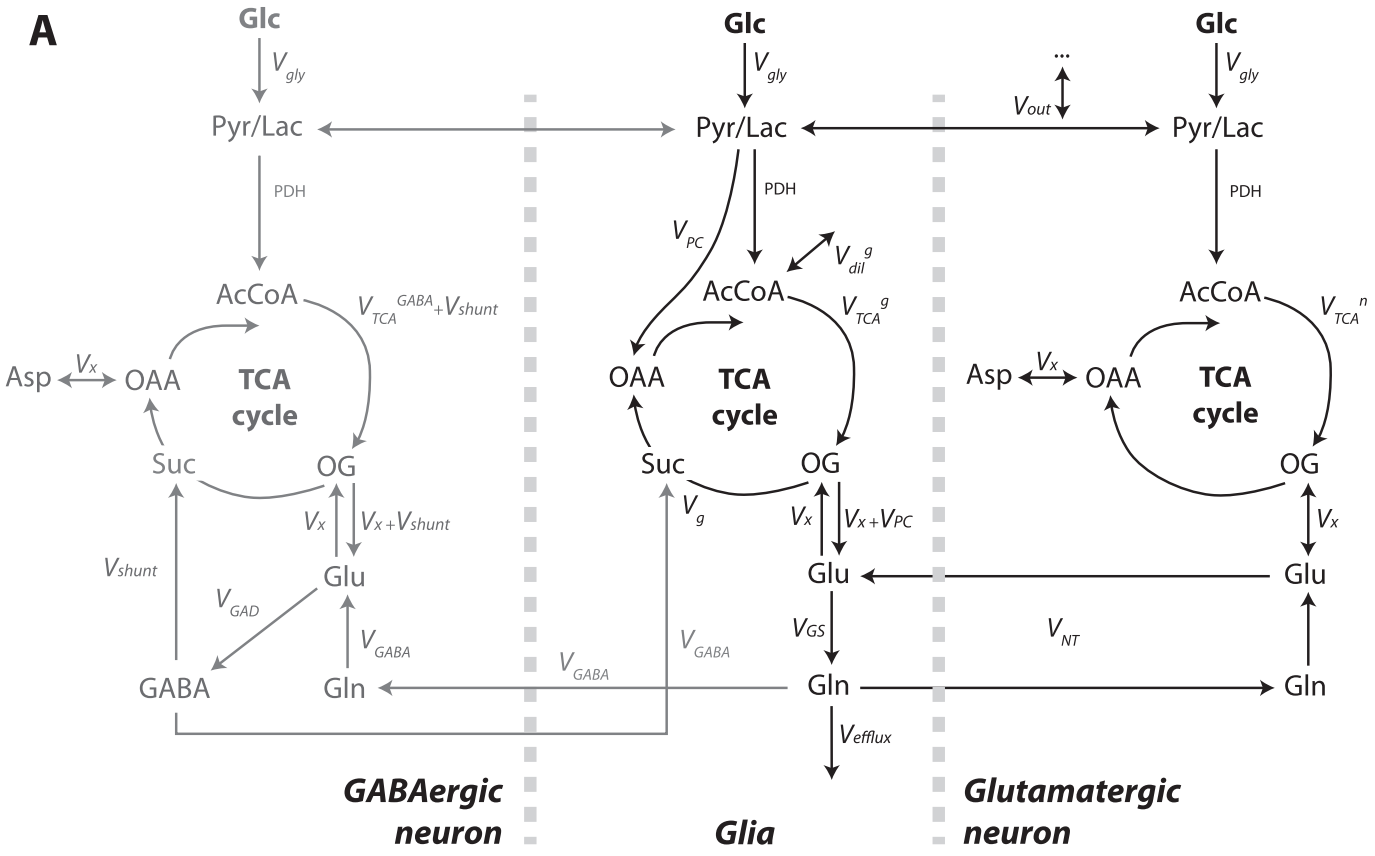

Fig. 3. (A) Three-compartment model of glucose metabolism accounting for trafficking between glial cells, GABAergic and glutamatergic neurons. The fluxes related to the GABAergic compartment (shown in grey) can be excluded from the modelling strategy leaving a two-compartment model for neurons and glial cells. (B) Labelling scheme deriving from the infusion of [1−^{13}C]glucose and [1,6−^{13}C]glucose with particular attention to labelling of glutamate (Glu), glutamine (Gln), GABA and aspartate (Asp) in the carbon positions usually reported in *in vivo* ^{13}C experiments with direct and indirect detection. Oxaloacetate (OAA), 2-oxoglutarate (OG) and other TCA cycle intermediates are usually in low

data, usually reaching high values of FE to increase ^{13}C concentration in the by-products of the metabolism under study and reach sufficient SNR for an accurate ^{13}C spectral quantification. For ^{13}C-glucose experiments, the desired plasma FE generally lies between 50 and 70% as a compromise between the need for higher ^{13}C concentration to improve sensitivity and the necessity to maintain the plasma levels of nutrients near physiological conditions. Typical infusion rates for euglycemic clamps are 9.96 mL/kg/h with a 20% mass/volume solution of glucose [47], which stabilises the plasma glucose level over time. A stable enrichment of the precursor in the plasma will lead to a progressive labelling of the downstream metabolites: the duration of the experiment is typically long enough to sufficiently characterize the labelling curve for each carbon position that is included in the model (Fig. 1C). Therefore, the required infusion time directly depends on the metabolism under investigation, on the desired level of details in the metabolic modelling of the data and on the cost of the substrate: as an example, when studying glutamate and glutamine turnover in the brain in order to characterize TCA activity in the separate neuronal and glial compartments under glucose infusion, 4–5 h of labelled glucose infusion would be desirable to reach a labelling steady state in C4, and high FE in C3 and C2 positions of glutamate and glutamine [19,22,23,29]. A longer time is needed for C2 and C3, since multiple cycling of the TCA cycle and the slower pyruvate carboxylase reaction characterize their build-up (Fig. 3B). However, such a long infusion experiment is not always compatible with the maintenance of a proper physiology under euglycemia or hyperglycemia, or with the tolerance of the subject, in particular for human studies. A good compromise has to be found for the experimental time, since an accurate measurement of the metabolites ^{13}C enrichment over a duration compatible with glutamate/glutamine turnover rates is essential to ensure accuracy and robustness in neuro-glial modelling, as distinct detection of C3 and C2 turnover curves is critical in distinguishing the glial compartment metabolism [43,48]. Dynamic experimental data of the temporal evolution of the ^{13}C-enriched metabolites (Fig. 1D) are integrated in a suitable metabolic model to estimate the fluxes of the metabolism under investigation by non-linear regression processes. The pool sizes of the metabolic model are determined from the total concentration of the metabolites quantified with ^{1}H MRS prior to the substrate infusion [29] or alternatively from analysis of brain extracts *ex vivo* [19,23,25].

Challenges particular to mice experiments mostly concern the inaccessibility to the arterial input function due to the limited blood volume as discussed above (1.5–2 ml). A standardized infusion protocol, designed on the base of bench experiments is an alternative to a direct measurement of the arterial input function that can be applied for metabolic modelling. Alternatively, specific ^{13}C detecting techniques such as ^{1}H-[^{13}C] MRS indirect detection [28,30,31], enable real-time measurement of the fractional enrichment of certain intermediates of brain glucose metabolism during the experiment. An example is the use of the measured FE of lactate in the ^{1}H-[^{13}C] MRS tissue voxel which can be used as an input function for the TCA cycle, representing the temporal evolution of pyruvate FE. This approach takes advantage of the fast exchange between pyruvate and lactate through lactate dehydrogenase (LDH) as compared with the TCA cycle rates [28]. In addition, it gives an input function which is closer to the processes of interest in terms of biochemical reactions network, the TCA cycle and neurotransmitter exchanges, accounting therefore directly for possible upstream dilutions in glucose uptake and glycolysis process.

2.1. Sensitivity and dependence upon B_0

Due to physical properties of the carbon nucleus, ^{13}C MRS is a relatively insensitive technique compared to ^{1}H and ^{31}P MRS. At thermal equilibrium, the NMR signal intensity depends on the total magnetization, which linearly depends on the applied polarization field B_0, according to the following relationship [49]:

$$M_0 = \left(\frac{\gamma h}{2\pi}\right)^2 \left(\frac{nB_0}{4kT}\right) \quad (1)$$

where γ is the gyromagnetic ratio, h the Planck constant, n the number of spins in the sample contributing to the magnetization build-up, B_0 the static magnetic field, k the Boltzmann constant, T the temperature of the sample and M_0 the macroscopic nuclear magnetization upon which the MRS signal depends. Sensitivity differences linked to the nucleus of choice are dependent on respective gyromagnetic ratios, yet an increase in the static magnetic field will be beneficial for all MRS techniques regardless of the detected nucleus. This linear dependency encouraged a steady increase in magnetic field strength in the last decades, especially for animal studies. An increase in B_0 also increases the difference in resonance frequencies of nuclei in different chemical environment, the chemical shift range [49], reducing peak overlap: this increased separation is of importance when simultaneously detecting molecules which have a similar carbon skeleton such as glutamate and glutamine. At 9.4 Tesla and higher fields, the C4, C3 and C2 resonances of glutamate and glutamine appear fully resolved when using direct detection techniques in the rat brain *in vivo* [22,50] while hydrogens linked to C3 and C2 of glutamate overlap with those of glutamine when applying ^{1}H-[^{13}C] MRS indirect detection [20,28]. However, recent acquisition of *in vivo* data at 9.4 and 14.1 Tesla with indirect detection approaches showed the possibility to distinguish between C3 resonances of glutamate and glutamine in the rat brain during the infusion of [U-^{13}C]Glc, [1,6–^{13}C]Glc at 14.1 Tesla and [2–^{13}C]Ace at 9.4 Tesla [21,30,51].

The equilibrium magnetization M_0 is generated by the spin population with a proportion of spins aligned with the external field increasing linearly with B_0. Due to Faraday's law of induction, the amplitude of the signal induced in the RF coil by the precessing magnetization depends on the Larmor precession frequency as follows:

$$S \propto \omega_0 M_{xy} \quad \text{with } \omega_0 = \gamma B_0 \quad (2)$$

where S is the NMR signal amplitude, M_{xy} the transverse component of the macroscopic magnetization (initially proportional to M_0) and ω_0 the Larmor precession frequency. In other words, a more intense electrical current is generated for higher Larmor frequencies for a given nucleus. Based on this effect and on Eq. (1) the signal S would theoretically be proportional to B_0^2 [52–54]. For *in vivo* applications, the sample reasonably constitutes the dominant source of noise detected by the same principle of induction.

concentration (below 1 mM) and therefore invisible in *in vivo* applications in the brain. Other abbreviations: glucose (Glc), lactate (Lac), pyruvate (Pyr), acetyl-CoA (AcCoA), glycolytic flux (V_{gly}), lactate dehydrogenase (LDH), pyruvate dehydrogenase flux (PDH), specific glial dilution from glial-specific substrates (V_{dil}^{g}), dilution of the lactate pool (V_{out}), pyruvate carboxylase flux (V_{PC}), total glial TCA cycle ($V_{TCA}^{g} = V_g + V_{PC}$), neuronal TCA cycle ($V_{TCA}^{n}$), transmitochondrial flux (V_x), neurotransmission flux (V_{NT}), glutamine synthetase flux (V_{GS}), glutamine efflux rate (V_{efflux}), GABAergic TCA cycle (V_{TCA}^{GABA}), glutamate decarboxylase flux (V_{GAD}), flux of GABA catabolism (V_{shunt}), GABAergic neurotransmission (V_{GABA}). The subscripts 1,2,3,… indicate which position in the carbon chain is labelled for a given metabolite.

For this reason, the intensity of the detected noise will also depend on B_0 linearly, resulting in a global linear dependence on B_0 for the SNR. Nevertheless, these considerations are not including all the factors influencing SNR in a MRS experiments: the entire experimental setup will influence the noise level, among which the noise generated by the RF coil and its efficiency in detection and transmission, the efficiency in the shimming techniques and hardware noise injection in the signal amplification processes, in addition to relaxation mechanisms and their dependency upon B_0. The dependency of the MRS signal on the natural abundance level of the ^{13}C isotope will not be discussed further, since this review focuses on experiments performed under infusion of ^{13}C-enriched substrates that are meant to increase the FE for the metabolites of interest well above natural abundance.

Considering the size of the brain of rodents and in particular, comparing rat brain with mouse brain, there is an obvious drawback on the sample size that will result in reduced signals in mice experiments. MRI morphometric measurements on rats above 200 g body weight estimate their total brain volume to around 1.7 cm^3 [55] while 8 weeks old mice brain imaged *ex vivo* resulted in an average of 0.4 cm^3 [56]. Furthermore, the mouse brain contains very similar complex cerebral structures in a smaller volume: this results in a higher density of interfaces between tissues and air-tissue with different magnetic properties, negatively affecting the B_0 field homogeneity. The higher tissue heterogeneity at equal volume is further amplified at higher field strengths, since differences in susceptibility between different adjacent tissues are proportional to B_0, resulting in a broadening of the linewidth. State of the art shimming techniques for rectification of field inhomogeneity become therefore critical for small volumes and/or strong B_0 and require at least 1st and 2nd order shimming that are commonly based on automated field mapping [57,58]. Rat experiments in which those techniques are implemented reported linewidths of 10–13 Hz for the water peak in a localized volume of 100 μL at 7 Tesla [20] while other authors measured 14–16 Hz in 180 μL at 9.4 Tesla [21] and 20–22 Hz in 144 μL at 14.1 Tesla [51]. Similar experiments performed in mice reported water linewidth of 24–28 Hz in 60 μL at 14.1 Tesla [28] whereas 27–30 Hz were obtained in 175 μL at 7 Tesla with manual localized shimming [27].

2.2. Direct and indirect ^{13}C detection

The molecules of biochemical interest detected in brain ^{13}C MRS are typically characterized by carbon nuclei linked to ^{1}H (NA >99.9%), ^{16}O (NA 99.8%) and ^{14}N (NA 99.6%) nuclei. ^{16}O has a magnetically inactive nucleus and does not interact with the ^{13}C nuclear spin. By contrast, heteronuclear scalar coupling between ^{1}H and ^{13}C generates peak satellites symmetrically placed around the ^{13}C main resonances, appearing as doublet/triplet patterns or combinations of them, due to the coherent nature of the spin-spin coupling effect [59]. Spectral splitting due to ^{1}H-^{13}C coupling noticeably lowers the SNR by complicating the spectral resonance pattern and lowering the individual peaks amplitudes (in addition to homonuclear ^{13}C-^{13}C splitting), making broadband ^{1}H decoupling particularly beneficial. Since the first ^{13}C MRS applications in cells and microorganisms [60–63] and rats [64,65], it appeared obvious that indirect detection of the ^{13}C nuclei through their neighbour ^{1}H nuclei would improve experimental sensitivity dramatically by making full use of the higher proton gyromagnetic ratio. As pointed out in the previous paragraph, the NMR signal depends on M_0 and ω_0, thus the gain in signal intensity for indirect detection depends on γ^3 [66]. The increase of noise induction upon the Larmor frequency will reduce the global gain in SNR to γ^2. The improvement would theoretically reach a 16-fold factor but these observations neglect the effects linked to ^{1}H-^{1}H coupling and multiplicity in the CH groups, as discussed elsewhere [42,66]. The overall spectral resolution is moreover influenced by the different linewidth obtained via direct ^{13}C detection compared with ^{1}H detection, due to the slower T_2 relaxation [67]. Moreover, opting for indirect detection techniques is made at the expenses of a narrow chemical shift range of the resonances of interest, resulting in strong signal overlap (that will preclude detection of metabolites of low concentration and ^{13}C isotopomer analysis), the need for water signal suppression methods and broadband ^{13}C decoupling. Globally, the choice between direct or indirect detection represents a trade-off between the amount of chemical information that will be available for metabolic modelling and the sensitivity (i.e. spatial and temporal resolution) needed in the experiment.

2.3. RF coil designs for in vivo ^{13}C MRS in rodents

Initial *in vivo* ^{13}C experiments in the late 80s and 90s made use of ^{13}C-^{1}H transmitter-receiver RF surface coils consisting in two concentric and co-planar loops [4,7,64,65,68–71], where the smaller one is tuned at the lower frequency (^{13}C) and the larger one to ^{1}H. Nowadays, ^{13}C-^{1}H surface coils are still largely preferred over volume coils due to the higher sensitivity achievable in the ^{13}C signal detection over a spatially localized region, mainly due to a better match between the coil sensitive volume and the sample size (filling factor) as well as the higher B_1 transmit field, of great interest for the large chemical shift range of ^{13}C resonances. Nonetheless, studies report ^{1}H volume coils used for heteronuclear decoupling in combination to ^{13}C surface coils: this setup strongly reduces inhomogeneities of the B_1 field at the ^{1}H frequency [27,72–74] and is especially suitable in human studies up to 3 Tesla, to address the requirements in terms of power deposition during decoupling.

Surface coils with co-planar concentric loops were proposed in the late 80s [75–77] and had successful applications *in vivo* especially at low fields. Their relatively limited performance in terms of SNR, due to interferences between the loops, became restrictive for high field applications. The same problems affected double-tuned surface coils that became obsolete nowadays [78,79]. In addition, the heteronuclear scalar coupling between ^{1}H and ^{13}C is relatively large ($^{1}J_{CH}$ = 120–170 Hz) and the related decoupling power also increases at higher field due to an increased decoupling bandwidth required for the same chemical shift range. Globally, the power requirements for decoupling depend on the square of the RF frequency (i.e. B_0^2) for a given bandwidth (in Hz) and on B_1^2 when increasing the decoupling bandwidth [80], becoming restrictive at high field strengths, both from the safety point of view and the available RF amplifiers [81].

Innovative RF coil designs were inspired by the need to meet safety guidelines [82,83] for human experiments, but they also influenced decades of applications in animal experiments. Single ^{13}C loop associated with a double ^{1}H-coil in quadrature configuration became the most popular set-up as surface coil for direct detection techniques [84]: the main advantage in humans consists in the higher filling factor due to an adapted geometry between the coil and the sample, when the voxel is located near to the surface of the head, which is a condition easier to meet in mice [85]. Moreover, the geometrical decoupling between the ^{1}H loops and the ^{13}C coil electrically isolates the two channels, resulting in optimal SNR during ^{13}C signal detection and avoids noise injections during ^{1}H decoupling. This is typically reinforced by adding bandpass filters on the ^{1}H and ^{13}C channels. The RF transmit power is also halved during ^{1}H decoupling by making use of the coil quadrature. Indirect detection can be achieved efficiently by using the same configuration with inversion of the ^{1}H and ^{13}C channels. The use of adiabatic pulses greatly increased the transmission efficiency of surface

coils over larger regions, overcoming the intrinsically high inhomogeneity in the B_1 field strength of these coils. First efforts were initially made in developing adiabatic full passage and half-passage pulses [86] that however cannot perform plane rotations, i.e. rotations are only effective for magnetizations that are collinear with the longitudinal axis. For this purpose, plane rotations adiabatic pulses were invented [87], which allow a constant rotation of any desired flip angle over a wide and symmetric bandwidth, despite the RF inhomogeneity [88], an advantageous condition for ^{13}C MRS *in vivo* applications.

RF coils are frequently home-made and adapted to the anatomy of the mice. ^{1}H coil loops required for mice experiments have diameters in the order of 12–15 mm [28–30], therefore covering the entire mouse brain for ^{1}H surface coils in quadrature configuration. The respective ^{13}C loop has usually a smaller diameter (9–10 mm), more comparable with the voxel size [28–30], which constitutes an advantage in terms of sensitivity since the ^{13}C loop is close to the localized region under study while the larger ^{1}H coil is commonly designed to simultaneously work for decoupling, ^{1}H localization, shimming and imaging the entire brain. All brain regions are virtually close to the coil when compared to a human surface coil, although sensitivity varies substantially along the coil axis due to B_1 inhomogeneity, which can nevertheless be mitigated with the use of adiabatic pulses for excitation. However, it could be expected that inhomogeneities in the B_1 field over the sample are reduced in mice due to the relative size of the coil compared to the brain: the Biot-Savart law dictates that the B_1 field on the loop axis has a penetration depth of approximatively a coil radius, so that theoretically the sensitivity would scale as r^{-1} when other sources of loss are neglected [89]. Since the ^{13}C loop diameter is usually comparable with the brain diameter in mice, the B_1 field will penetrate more than in the human brain where the size of the loop (80–100 mm [90]) is much smaller than the diameter of the brain.

The size of RF coils compared to the animal or human head is of great influence to the source of noise as well, even if the same design is used. Sample losses are indeed dominant in RF coils for human applications, where the localized signal usually comes from a relatively small region while the coil is loaded by the whole head. Conversely, all sources of losses are equally important while detecting ^{13}C signal in small rodents, where the total ^{13}C signal is reduced due to the smaller volumes but the sample losses are reduced as well: hardware elements (coil, capacitors and transmission line) and the sample equally contribute to the noise level [85]. Cryogenic coils are commercially available and represent a solution to lower the noise sources coming from the coil and preamplifier. Nevertheless, cryogenic coils are maintained under a strong temperature gradient between the chilled circuitry and the surface close to the sample, impeding a close proximity to the mouse head that can be accomplished with room temperature coils [41].

3. Metabolic flux analysis

The strong asset of ^{13}C MRS in studying brain metabolism mostly resides in the possibility of quantifying metabolic fluxes of a range of biochemical reactions involved in the metabolism of the injected labelled substrate. This is made possible by the high level chemical specificity of ^{13}C MRS, as compared to radionuclei-based labelling studies. The chemical shift of ^{13}C resonances not only carries information on which molecule species is labelled, but also at which position of the carbon molecule backbone. Distinguishing between labelling levels in the precursors and different by-products of given biochemical reaction chains enables insight into brain energy metabolism and neurotransmitter cycling. This complex set of information is measured dynamically over time and further analysed with a suitable mathematical model, summarizing the key neurochemical reactions involved in the labelling of the measured molecules. The free parameters of the model, typically a set of metabolic fluxes, are adjusted through a regression process in order to get the labelling model functions that best describe the *in vivo* measured kinetics, resulting in a set of characteristic flux values. This complex set of quantitative information on metabolism makes the whole effort against the poor ^{13}C sensitivity issue worthwhile. Another technique which greatly enhances ^{13}C signal *in vivo* is the employment of hyperpolarized substrates. However, sophisticated MFA is trickier to apply in this context, since rather than absolute ^{13}C metabolite concentrations, signal ratios of different ^{13}C peaks are obtained, subject to polarization decay by relaxation and RF excitation.

The most common modelling approach in ^{13}C MRS is compartmental modelling where the organ, tissue or any biological unit under study is depicted as an ensemble of distinct subunits where the label enters and can move through a defined metabolic pathway [91,92]. Nowadays metabolic models for brain kinetics frequently include two or three compartments accounting for cell-specific metabolism: most of the models describe neuro-glial interaction while fewer attempted to discern between GABAergic and glutamatergic neurons [21,93,94], mostly *ex vivo* [95,96]. On the other hand, spectra acquired with indirect detection techniques are typically analysed with a one-compartment approach given the frequent overlap between C3 and C2 positions of glutamate and glutamine [28,30] and the induced limitations on biochemical information.

In compartmental modelling, the biological system under study is divided in a finite number of compartments and metabolic pools, representing different molecules and carbon positions within these molecules, connected by metabolic fluxes (Fig. 2A) [43]. A compartment is characterized by an ensemble of metabolic pools which behaves homogeneously in a tracer study since it is governed by a characteristic structure from the chemical point of view. A pool is a portion of the compartment characterized by an homogeneous kinetics (Fig. 2B), meaning that any product entering with an influx is instantaneously mixed and indistinguishable [97,98], or in other words each molecule of a given pool has the same probability of leaving it through an efflux. The metabolic fluxes define the relevant chemical reactions or set of chemical reactions as well as the transport processes of the molecules across cellular and tissue membranes, such as the transport of the substrate through the BBB from plasma to the tissue compartment. An accessible compartment is used for the introduction of the labelled substrate of choice (i.e. plasma compartment) and its fractional enrichment over time is known as input function. The system being isolated, it is subject to several constraints dictated by mass-balance equations. Metabolic steady state is usually assumed, which means that total concentrations of the metabolic pools as well as metabolic fluxes are constant throughout the infusion experiment. Studies tracking the time evolution of the pool sizes, as possible with ^{1}H-[^{13}C] MRS, have shown that the assumption of constant metabolic pool sizes is admissible for studies with infusion of ^{13}C-glucose [3,48], while it might need refinement for other substrates, such as for [2–^{13}C] acetate, where an increase in glutamate was measured [99].

The following paragraph will illustrate how differential equations can describe metabolite kinetics in a single-pool and more complex models. The fitting procedure and Monte Carlo simulations to evaluate the precision of the parameters determination will be briefly presented.

3.1. Kinetics of a single pool

The labelling pool is the smallest unit of a compartmentalized

model. For the sake of simplicity, a single pool with one incoming flux and an efflux will be considered with the analytical representation of its labelling time course as an illustrating example. A generalization to a generic number of labelling pools and fluxes will then be described.

In ^{13}C labelling experiments, the total concentration of labelled and unlabelled metabolite defines the pool size. Each metabolite is the product (P) of one or multiple chemical reactions in the system. The variation over time of the total product concentration corresponds to the difference between the incoming flux (V_{in}) and the efflux (V_{out}), following the mass conservation principle [43,48]:

$$\frac{dP(t)}{dt} = V_{in} - V_{out} \tag{3}$$

The metabolic steady state assumption implies $\frac{dP(t)}{dt} = 0$, hence:

$$V_{in} = V_{out} \tag{4}$$

Once the labelled substrate is administered through the plasma, the concentration of labelled product (P^*) will start increasing. The ratio between the labelled form of the product and its pool size [P] is defined as the FE of the pool. The variation in the labelling concentration of the product of the product P is governed by the labelling equation:

$$\frac{dP^*(t)}{dt} = \frac{S^*(t)}{[S]}V_{in} - \frac{P^*(t)}{[P]}V_{out} \tag{5}$$

where each flux is multiplied by the time-dependent FE of the metabolite in its compartment of origin. The function $\frac{S^*(t)}{[S]}$ for the substrate injected in the plasma (i.e. the input function of the experiment) is frequently determined by serial blood sampling or imposed by *a priori* knowledge, whereas the fractional enrichment of the product $\frac{P^*(t)}{[P]}$ is measured from the *in vivo* ^{13}C MRS data. With the metabolic steady state condition, the differential equation can be solved and the solution adjusted to the measured enrichment time course for the determination of V_{in} and V_{out}. In this case, the situation reduces to the quantification of a single parameter since $V_{in} = V_{out}$.

In a general scheme (Fig. 2B), the pool i of the biological system under study will be characterized by n fluxes that will generate an influx and m generating an efflux.

The labelling equation for a single pool is a first order linear differential equation that can be solved analytically in the general form [43]:

$$P^*(t) = \int_0^t V_{in}\frac{S^*(t)}{[S]}\exp\left(\frac{V_{out}}{[P]}\left(t' - t\right)\right)dt' \tag{6}$$

This equations can be further simplified by applying the condition of metabolic steady state (i.e.$V_{in} = V_{out}$), and employing the easiest shape for the input function, namely a step function. In this case, the FE of the substrate will be nearly zero at $t = 0$ and it will raise to a constant level $\frac{S^*}{[S]}$ at $t > 0$. The analytical form of the labelling curve in the product pool will simplify to:

$$\frac{P^*(t)}{[P]} = \frac{S^*}{[S]}\left(1 - exp\left(-\frac{V_{in}}{[P]}t\right)\right) \tag{7}$$

meaning that the FE will increase exponentially and eventually reach a plateau at steady state around $\frac{S^*}{[S]}$. The rapidity with which the curve will reach steady state directly depends on the influx V_{in} and be inversely proportional to the pool size [P]. A common case when designing a metabolic model is the presence of a dilution flux in the pool, which is a constant contribution to the molecule by unlabelled sources (V_{dil}; Fig. 2C). Under these circumstances, the mass balance equation has the form:

$$\frac{dP(t)}{dt} = V_{in} + V_{dil} - V_{out} = 0 \tag{8}$$

It follows that $V_{in} = V_{out} - V_{dil}$. The labelling in the product pool is therefore given by the following expression:

$$\frac{P^*(t)}{[P]} = \frac{S^*}{[S]}\frac{V_{out} - V_{dil}}{V_{out}}\left(1 - exp\left(-\frac{V_{in}}{[P]}t\right)\right) \tag{9}$$

In this case, the labelling curve will level off to the value of FE $\frac{S^*}{[S]}\frac{V_{out}-V_{dil}}{V_{out}}$ at steady state, decreased by the fraction $\frac{V_{out}-V_{dil}}{V_{out}} < 1$ compared to the example in absence of dilution.

In a more complex system made of N interconnected metabolic pools, each pool will generally receive labelling/dilution from n incoming fluxes and be drained through m fluxes (Fig. 2B). The whole system is therefore described by a set of N coupled differential equations of the following form:

$$\frac{dP_i^*(t)}{dt} = \sum_{j=1}^{n}\frac{S_j^*}{[S_j]}V_{in}^j - \sum_{k=1}^{m}\frac{P_i^*}{[P_i]}V_{out}^k \tag{10}$$

where $i = 1, \ldots, N$.

3.2. [1–^{13}C] and [1,6–^{13}C]glucose metabolism in neurons and glial cells

The neuro-glial compartment model for energy metabolism is an example of a complex system of metabolic pools connected by metabolic fluxes (Fig. 3A). [1–^{13}C]glucose or [1,6–^{13}C]glucose infusions are the most common substrates used in the study of brain energy metabolism that label glutamate and glutamine downstream of oxidative metabolism and neurotransmission. The chemical shift range commonly accessible potentially allows the detection of C4, C3 and C2 resonances of glutamate and glutamine over time: C4 curves are usually detected separately while C3 and C2 positions appear frequently overlapped (Glx) depending on the sensitivity available with a given magnetic field and on the technique of detection. The wide chemical shift range of direct ^{13}C detection enables typically the complete separation of the different labelled carbon positions [22,27,29,93,100–102].

As summarised in Fig. 3B, the ^{13}C at the positions C1 and C6 of glucose is transferred to the C3 of pyruvate before entering the TCA cycle. The labelling curves comprise glutamate and glutamine located in both neurons and astrocytes: glutamate is mostly attributed to neurons and glutamine is mainly located in astrocytes, reported by immunohistochemical staining [103,104]. Moreover, total glutamate concentration is usually about twice higher than glutamine [105,106] and the neuronal TCA cycle rate is typically higher than the glial TCA cycle rate. In other words, most of the ^{13}C label is transferred in neurons, which makes the ^{13}C turnover curves particularly sensitive to neuronal metabolism. The first carbon position being labelled is glutamate C4 followed by glutamine C4. Since glutamate is attributed almost entirely to neurons, the C4 labelling curve (Fig. 1D) carries the information on the neuronal TCA cycle (V_{TCA}^{n}) and the transmitochondrial flux (V_x) while the curve is rather insensitive to the neurotransmission flux (V_{NT}) that carries additional labelling from the glial compartment [107]. Conversely, glutamine is labelled to a greater extent from the larger neuronal glutamate pool and the shape of its FE curve is more sensitive to V_{NT}, which has however a reduced impact on the first

part of the curve [107]. The FE at steady state for glutamate C4 is commonly lower than FE of glucose (Fig. 1D), meaning that a dilution or a net loss of labelling must occur: this is usually justified as a consequence of glucose utilisation for non-oxidative purposes, lactate exchange with the extracerebral compartment or incorporation of unlabelled substrates other than glucose [108].

If no other cell-specific flux would be present, the C4 curves of glutamate and glutamine would reach the same FE at steady state. C3 and C2 curves would appear equally labelled, since there is the same probability of labelling the two positions during the second and further cycling of TCA cycle. However, the relative FE of the different carbon positions is not the same in glutamine and glutamate (Fig. 1D) reflecting distinct kinetics in the glial and neuronal compartments. At first, a dilution flux is present in the glial compartment due to the incorporation of glia-specific substrates such as acetate, fatty acids and ketone bodies, decreasing the glutamine label equally in all positions. Moreover, the anaplerotic activity of pyruvate carboxylase has the effect of increasing the FE at the position C2 while diluting the position C3, by simultaneously introducing a ^{12}C. The glutamate pool (mostly neuronal) is less affected by the increase in the C2 FE since the neuronal mitochondrial metabolism has a higher impact on its labelling. Therefore, the C3 and C2 curves of glutamate are typically close together while FE in glutamine C2 is typically higher than the enrichment in C3.

Detection of GABA labelling curves theoretically allows the distinction of GABAergic neurons in the modelling strategy (Fig. 3A), while aspartate C3 and C2 curves can be included in both models in order to reach a more precise flux estimation.

In the following paragraph we explain how flux estimation is usually performed, how the number of estimated parameters and their precision is influenced by the noise, the number of measured labelling curves and their temporal resolution.

3.3. Flux estimation

For the flux estimation, a labelling equation is defined for each metabolic pool of the system, where the functions $\frac{P_i^*(t)}{[P_i]}$ are determined experimentally and the parameter V_i are estimated. However, more generally, some labelling curves can be undetermined before modelling or insufficiently characterized due to a poor temporal resolution, which in turns can require some parameters to be fixed by several constraints or *a priori* knowledge. The complexity of the model and the measureable metabolic parameters are in tight connection with the number of accessible labelling pools in the biochemical reaction chain under study. Globally, a higher number of experimental labelling curves will increase the robustness of the modelling process and the number and precision of estimated parameters [107].

Parameter optimization in ^{13}C metabolic modelling is often achieved by solving the differential equations numerically by least-square regression [26,98,109]: briefly, the method will try to find the most appropriate set of parameters that allows minimizing the sum of the squared differences (e.g. χ^2) between the labelling curves produced by the model with the given fluxes and the experimental curves. Given an experimental turnover curve $y(t_i)$ discretely determined at M time points t_i and a set of parameters $V_1, \ldots, V_N$ that generate the model simulated function $f(V_1, \ldots, V_N, t_i)$, the cost function of the regression is given by Ref. [26]:

$$\chi^2 = \sum_{i=1}^{M} [f(V_1, \ldots, V_N, t_i) - y(t_i)]^2 \quad (11)$$

The process will be repeated iteratively until reaching the estimation of an appropriate set of parameters corresponding to the minimum of χ^2 that will correspond to the "best" fit. However, the analysis might fall into a local minimum [26] or a very broad minimum, in particular when the system is underdetermined. A first control of the accuracy of the analysis is usually performed with the systematic inspection of the residuals. When the residuals of a fit show a clear pattern, it might conceal a bias or incompleteness in the modelling strategy, which needs revision. Additionally, the estimated results might be strongly influenced by specific assumptions or fixed parameters [42,48]. The sensitivity of the estimated parameters upon the assumptions is often assessed by observing their change when varying the constraints within a reasonable range.

Another important aspect in ^{13}C MRS is the noise level and its impact on the parameter estimation: up to now we presented the problem of parameter estimation, neglecting the existence of a noise source in the experimental data and how its intensity affects the estimation. As a matter of fact, the algorithms dedicated to least square fitting provide an estimation of the uncertainties that are based on the assumption of a "vanishingly small" noise in the experimental data [26] ($\frac{stdev(Signal)}{Signal} \ll 1$), based on the covariance matrix. As previously discussed, given the challenging nature of the *in vivo* ^{13}C detection, this assumption is not always valid, leaving space for the implementation of a method that is able to assess the impact of noise on the analysis. A common approach is to use the Monte Carlo (MC) simulations [110,111] which are based on artificial datasets with similar characteristics to the experimental data, with different realization of noise of same power. A first noise-free dataset is generated from the estimated fluxes, $V_1, \ldots, V_N$ obtained from the best fit of the experimental data. A set of experimental curves (typically several hundreds) is then generated with the addition of a specific noise realization to each noise-free turnover curve, with the same noise characteristics as the experimental data (SD or power). By fitting the artificially generated data sets with the same metabolic model, the method will generate a probability distribution for each estimated parameter, reflecting the variability of the flux determination as a function of the experimental noise variation. The SD or any further statistical measure on the flux probability distributions carries the information on each flux precision and its reliability in the metabolic analysis. Other important features that can be obtained from MC analyses are covariance or correlations of the calculated fluxes, pointing to their relative independence in the parameter optimization process. Strongly correlated fluxes may indicate a need for simplification by a reduction of the number of free parameters, typically based on *a priori* knowledge from previous biochemical experiments.

Ideally, when spectra are measured dynamically, every point should be measured with the same precision, or in other words, every experimental point has the same "weight" in the fitting procedure. However, precision in the determination of ^{13}C concentration of a given carbon position could vary along the experiment, especially for low concentration metabolites at the beginning of the substrate infusion. In this case the least-square fitting procedure can be done through a weighted cost function, such as [112]:

$$\chi^2 = \sum_{i=1}^{M} w_i \left[f(V_1, \ldots, V_N, t_i) - y(t_i)^2 \right] \quad (12)$$

where the weight w_i applied to each experimental point is usually determined from the precision in the estimation of labelling concentration at the point t_i.

^{13}C labelling experiments typically detect a set of uptake curves simultaneously. Therefore, the fitting procedure implies the simultaneous least-square regression for the different labelling curves. In practice, detection of certain carbon positions over time will be more challenging due to the relatively low FE of certain

metabolite carbon positions or due to overlap with other carbon peaks. As a result, certain curves are determined with a lower precision, which will generate a larger contribution to the cost function. Dynamic data of such curves can be integrated in the model with a corrected impact to flux estimation by attributing a weight to each of the L labelling curves measured during the experiment [113]:

$$\chi^2 = \sum_{j=1}^{L} \sum_{i=1}^{M} w_{ij} \left[f_j(V_1, \ldots, V_N, t_i) - y_j(t_i)^2 \right] \quad (13)$$

It is to note that the cost function is weighted by the square of the difference between the measured curves y_j and the simulated functions f_j, not by their amplitude. So, a high SNR curve (such as GluC4) will not necessarily contribute more to the cost function than a low enrichment curve, such as GlnC2. It is the amplitude of the dispersion of the experimental points around the model functions that contributes to the cost function value.

We typically measure low FE curves (such as the C2) with higher noise level than e.g. the C4, due to the more difficult spectral quantification, which would improperly contribute more to the cost function. Weighted regression enables then to correct for the different SD of the measured points/curves and work with an unbiased cost function. This method also enables equivalent fitting results of FE turnover curves or ^{13}C concentration curves, since a concentration scaling of the corresponding curves (and noise) is adjusted in the cost function.

An unbiased weight attributed to each time point i of the curve j is defined by the inverse of the variance of each curve time point:

$$w_{ij} = \frac{1}{SD_{ij}^2} \quad (14)$$

4. *In vivo* ^{13}C brain MRS: chasing a new standard in ^{13}C sensitivity

Historically, advances in *in vivo* brain ^{13}C MRS in animals and humans have been highly interrelated: in the following paragraphs the connection between the technical advances of note in the field of ^{13}C MRS will be highlighted, as well as their impact on *in vivo* ^{13}C MRS in humans and in rodents, namely on spatial resolution, metabolite detection and consequent improvements in metabolic flux modelling.

4.1. An historical perspective: ^{13}C brain MRS in its infancy

In the early '70s ^{31}P MRS was frequently used in living microorganisms to study several phosphate-containing metabolites. Interesting characteristics of these measurements, such as non-invasiveness and direct access to metabolite kinetics drew attention on the possibility to use the same NMR techniques with ^{13}C, aimed at studying carbohydrate metabolism. The first systematic study on the occurrence of the ^{13}C isotope was actually published in 1939 [114] well before the discovery of the NMR effect and thus, the advent of Fourier transform techniques in 1966 [115]. However, highly enriched compounds were not available at that time. Therefore, research focused on the radioactive ^{11}C and ^{14}C compounds. First ^{13}C natural abundance spectra were shown by Lauterbur in 1957 [116] while the first studies on yeast, cells and mitochondria [117–120] were made feasible with the use of FT and newly available ^{13}C enriched compounds [121].

Glucose metabolism was the first to be examined with ^{13}C MRS experiments in yeast [118] and *E. coli* [122], the latter showing time courses of by-products related to glucose catabolism. Few years later a first attempt of modelling glucose uptake was made on data collected from yeast cells fed with [1–^{13}C] and [6–^{13}C] glucose with a Michaelis-Menten kinetic model [123], while main chemical reactions of the TCA cycle were estimated for the first time in cardiac tissue *in vitro* [11]. Up to this point, computational methods were still immature and magnetic fields available for research reached approximately 2 Tesla. Moreover, techniques of 3D localization were not yet established, hence the appearance of lipid signals were often interpreted as free mobile lipids. In *in vivo* animal experiments, the sensitivity issue in the small rat or rabbit brain was often solved by putting the surface coil in direct contact with the skull by retraction of the skin [64,68] and by opting for indirect detection techniques [64].

In the early 90's, ^{13}C MRS was then applied to human volunteers: infusion of labelled glucose in euglycemic and hyperglycemic conditions allowed to detect dynamic data from glutamate enrichment through TCA cycle at sufficient FE [3,70,71,124]. Finally, the introduction of automated shimming [57,58] and 3D localization allowed a great improvement in spectral resolution: for the first time, ^{13}C localized MRS identified lipid resonances as a contribution from subcutaneous fat rather than intracranial mobile lipids [71]. Few experiments were performed with natural abundance signals [2,5,6] revealing the possibility of quantifying several molecules involved in brain metabolism, such as glucose and myo-Inositol, that were not accessible at the time, given the low spectral resolution available in ^{1}H MRS. The sudden enhancement in spectral resolution opened a window for the study of brain compartmentation from the distinct detection of glutamate and glutamine in the brain *in vivo* [4,58].

From here on, magnetic field strengths available in clinics and animal research field have been experiencing a steady increase: although the increase in B_0 field is directly connected with sensitivity by reducing peak overlap, researchers had to cope with higher power demand for broadband decoupling and spatial localization, which is essential in *in vivo* applications. Limitations in power depositions are particularly strict for human subjects and required specific attention in developing new strategies in coil development and sequence design as discussed above.

4.2. Rodent models for ^{13}C MRS in vivo

Rodents are widely employed in preclinical research on brain diseases, thanks to their proximity to the human genome and even more similarities to the human immune system, which supports the development of similar pathologies and reproduces treatment response [125]. Other characteristics, such as the possibility to develop genetically engineered species among mice and rats opened the way to reproducing disease models that preserve the same genetic aberration of the human counterpart [125].

In this context, MR techniques offer a non-invasive approach to investigate metabolism in healthy animal models and in models of brain diseases *in vivo*, preserving brain cells in their natural microenvironment, namely brain parenchyma and BBB, which is specifically known to influence drug response. *In vivo* ^{13}C MRS requires the injection of expensive labelled substrates, which makes the use of small animal species of advantage in terms of amount of tracer needed per subject. Besides this, rodent animal models provide easier handling procedures and are less expensive to purchase and maintain than other typical research animals, such as primates. Although mice are the most widely used animal model in biomedical research, MRS studies of low-gyromagnetic ratio nuclei have to date focused mainly on the rat brain due to its larger size (~1200 mg vs ~400 mg [126]), facilitated surgical interventions and maintenance of normal physiology.

4.3. State of the art in vivo ^{13}C MRS in the rat brain

First feasibility studies of *in vivo* brain ^{13}C MRS were carried out on rats [64,65] with indirect detection techniques shortly followed by several human studies: after the first attempt of measuring glucose uptake and metabolism in human subjects [4,71], several *in vivo* measurements in rats were performed at 7 Tesla [18,19,127] to obtain a more detailed measurement of brain metabolism using direct ^{13}C detection, providing more distinguishable metabolite resonances. All these measurements were performed with surface coil detection only. Lipid resonances were eliminated by subtraction of a spectral baseline acquired prior to substrate infusion. Spectral quality suffered from a relatively large linewidth (40–60 Hz on water signal [18,127]). Introduction of improved localized shimming procedures on first and second order coils [58,128] and localization strategies based on ISIS scheme in human studies [129,130] improved dramatically the spectral resolution on the metabolites (linewidth <10 Hz) allowing the measurement of extended time courses of glutamate and glutamine at the position C4 [131] even at low field strength [129]. Finally, distinct measurements of C4, C3 and C2 amino acid resonances upon infusion of [1–^{13}C]glucose in humans opened the way to model brain metabolism with a two-compartment approach, which accounts for neuro-glial trafficking [100,127]. Similar experiments were performed in rats at 9.4 Tesla in typical volumes of 510 μL [102]: turnover curves of glutamate and glutamine C4 and C3 together with aspartate C3 were included in the model, while data on C2 turnover curves of glutamate and glutamine were not reported. Metabolic flux analysis of neurons and astrocytes was similarly investigated in rats with [2–^{13}C] and [5–^{13}C]glucose at 7 Tesla [19] although in unlocalized spectra with lipid baseline subtraction.

Regional glucose metabolism in rats was later assessed at higher spatial resolution (up to 25 μL) achieved with indirect detection at 7 Tesla in the rat brain [20]: a two compartmental approach in the modelling strategy was kept to model the distinct C4 resonances and the sum of C3 peaks for glutamate and glutamine, including *a priori* knowledge imposed on glial TCA cycle and anaplerotic flux. GABAergic metabolism was finally implemented in a three-compartment model (Fig. 3A) for the first time by integrating *ex vivo* and *in vivo* data measurements with direct detection in a 360 μL voxel [101]. Similar experiments under infusion of [2–^{13}C] acetate could distinguish between C3 peaks of glutamate and glutamine in a 196 μL volume at 7 Tesla [132]. Again, labelling curves determined *in vivo* were supplemented with *ex vivo* data on C3 peaks to allow the use of a two-compartment model.

Detection of *in vivo* time courses of GABA peaks remained challenging at 7 Tesla due to the relatively low concentration of this metabolite and spectral overlap. By raising the field strength to 9.4 and 14.1 Tesla, an increasing number of by-products were measured *in vivo*: for the first time distinct detection of C4 and C3 time courses of glutamine and glutamate were reported with indirect detection technique during infusion of [2–^{13}C]acetate [21,51] in relatively small voxels (144–180 μL). Moreover, since acetate is a substrate selectively taken up by astrocytes, it enters the glial TCA cycle at the level of acetyl-CoA and labels the neuronal glutamate through the glial glutamine pool (Fig. 3A). The specific label flowing from the astrocytic compartment increases the sensitivity by measuring the glial TCA cycle and neurotransmission with a two-compartmental model [99].

Direct ^{13}C detection in the rat brain remained confined to larger voxels compared to the standard reached with indirect detection (~300 μL for resolved C4, C3 and C2 of Glu/Gln): recent studies could take advantage of larger spectral dispersion at ultrahigh fields finally measuring complete *in vivo* time courses of C4, C3 and C2 positions of glutamate and glutamine, as well as a large cohort of by-products linked to glucose metabolism [22,23] as previously demonstrated [50]. Dynamic data collected over 5 h of [1,6–^{13}C] glucose were treated either with a neuroglial modelling approach or a three-compartment model (Fig. 3A) to discern GABAergic and glutamatergic neuronal activity.

To date, ^{13}C MRS in rats has reached relatively good standard in spatial resolution in ultrahigh field: experiments mainly reflect metabolism of the cortex and hippocampus which are closer to the brain surface and therefore easier to detect with surface coil configurations. Studies in healthy rats contributed noticeably to the understanding of brain function in terms of substrate consumption and metabolic rate assessment for specific cell populations, as compared to the first measurements of global TCA cycle rates in the rat brain [65,133]. Direct and indirect detection techniques contributed to gain a quantitative understanding of GABAergic and glutamatergic neurotransmission under physiological conditions.

4.4. ^{13}C MRS in the mouse brain in vivo

Although *in vivo* ^{13}C MRS in rats contributed to elucidate basic mechanisms of brain metabolism with an appreciation of cell-specific roles in neuroenergetics, the further application of this technique to mice is of great interest. In fact, a wider variety of genetically engineered species are available among mice. These models are employed in biomedical research to replicate genetic aberrations that are linked to pathogenesis and mechanisms of many human diseases. Mice are the most used animal models in this field and a more extensive literature on *in vitro* and *in vivo* studies is available.

Given the limitations in ^{13}C detection *in vivo* in small volumes, ^{13}C MRS in mice was at first applied to tissue brain extracts with indirect detection [95]: these results gave a quantitative appreciation of neuroglial metabolism with their respective regional differences and distinction of GABAergic and glutamatergic neurotransmission. A first proof of concept of the feasibility of *in vivo* detection was made at 7 Tesla with a direct detection sequence applying ^{1}H polarization transfer to ^{13}C, combined to ^{1}H broadband localization [50] in a volume of interest of 175 μL [27]. Complete time courses of glutamate and glutamine at the positions C4 and C3 were reported upon infusion of [1,6–^{13}C]glucose. These results were later compared by Sack et al. with *in vivo* acquisition performed with a surface coil cooled at cryogenic temperatures [41] on mice infused with [1–^{13}C] Glc: this technology allowed distinct detection of C4, C3 and C2 resonances of glutamate and glutamine together C4 and C2 peaks of GABA. Position C3 of GABA was hidden below noise level in dynamic acquisitions with a temporal resolution of 12 min. The authors reported that theoretically, an improvement in the SNR of 6.5 could be reached with the cryo-technique if acquiring spectra in the same experimental conditions as in Ref. [27] (with polarization transfer and infusion of [1,6–^{13}C] Glc).

More recently, ^{13}C MRS has been applied with increased spectral dispersion and SNR at 14.1 Tesla in a voxel of 112 μL in the central brain [29] by infusing [1,6–^{13}C]glucose: this finally allowed the detection of complete time courses of C4, C3 and C2 peaks of glutamate and glutamine and a wide range of glucose by-products during 5 h of infusion. Complete time courses of glutamate and glutamine were integrated in a two-compartment model for neuroglial metabolism reaching a quantitative understanding of the respective compartments by determining TCA cycle rate in neurons (V_{TCA}^{n}) and astrocytes (V_g), pyruvate carboxylase activity (V_{PC}), transmitochondrial flux (V_x) and neurotransmission (V_{NT}).

Higher spatial resolution was achieved with ^{1}H-[^{13}C] MRS at 14.1 Tesla in a voxel of only 60 μL placed in the frontal brain (cortex and striatum): measurements included the C4 position of glutamate

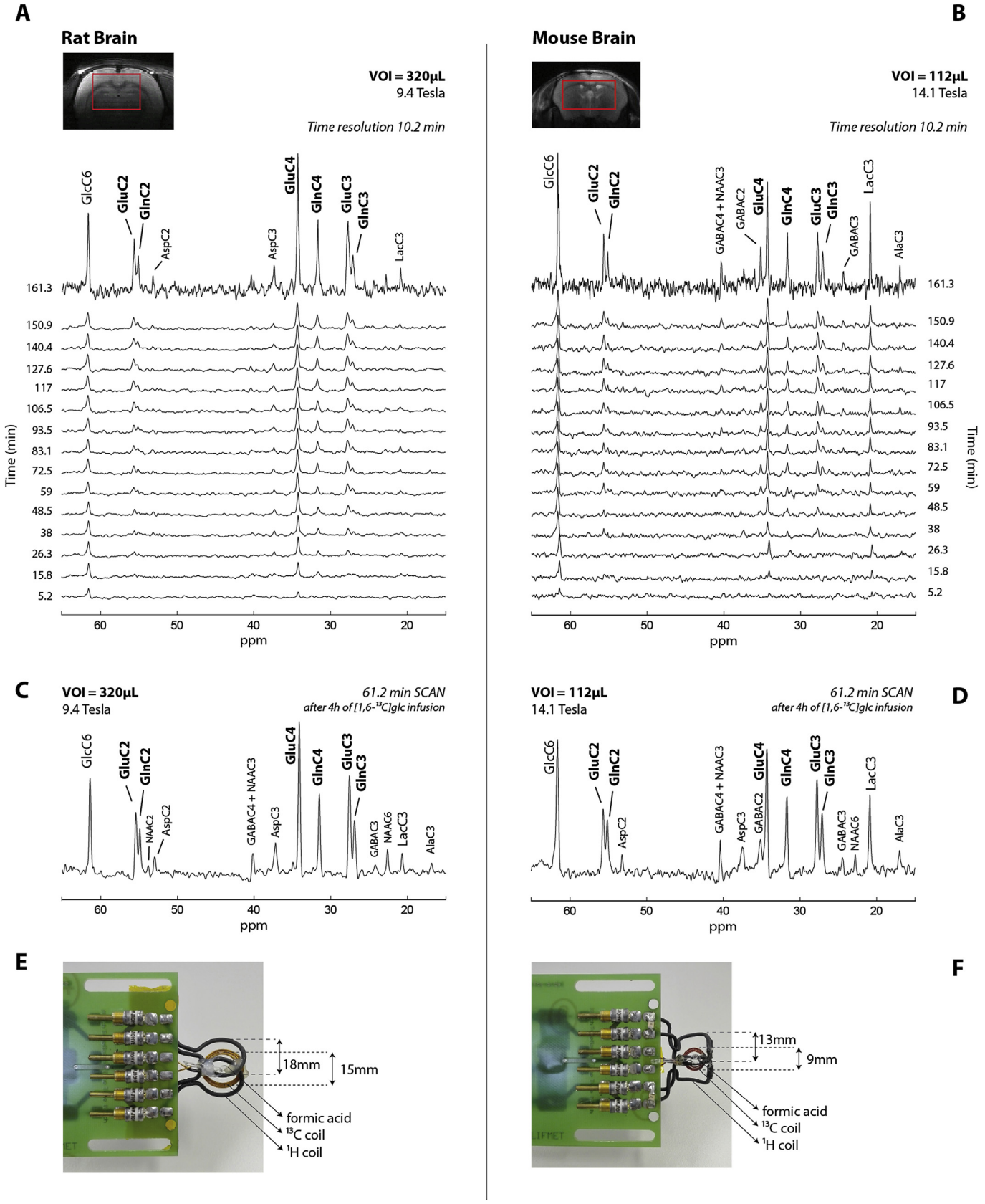

Fig. 4. *In vivo* ^{13}C direct detection in the rat (A–C) and mouse brain (B–D) at 9.4 and 14.1 Tesla respectively, during infusion of [1,6–$^{13}C_2$]glucose. Direct detection was achieved with semi-adiabatic DEPT polarization transfer sequence [50]. Rat spectra were acquired in a 320 µL voxel ($5 \times 8 \times 8 mm^3$) including the cortex and part of the central brain and mouse spectra in 112 µL ($3.6 \times 6.9 \times 4.5$ mm^3) placed in a central region. Both animals were infused with a 5 min exponentially-decaying bolus of 99%-enriched [1,6–$^{13}C_2$]glucose followed by 5 h of continuous infusion with 70%-enriched [1,6–^{13}C]glucose. Dynamic acquisitions (A–B) at temporal resolution of 10.2 min starting after the bolus (lb = 20 Hz between 5 and 150 min; lb = 10 Hz at 160 min). Steady state spectra (C–D) are acquired in the same regions for 61.2 min after 4 h of [1,6–$^{13}C_2$]glucose infusion (lb = 20 Hz). Mouse spectra show a distinct metabolic profile linked to the predominance of the striatum in the volume of interest, such as pronounced GABA and lactate peaks, due to their relatively large concentration in this region [105]. To follow the fate of ^{13}C-glucose through the different by-products, please refer to Fig. 3B. ^{13}C-[^{1}H] quadrature coils used for the spectra acquisition in rats and mice are shown respectively in E and F. Abbreviations: volume of interest (VOI), glucose (Glc), glutamate (Glu), glutamine (Gln), N-acetylaspartate (NAA), aspartate (Asp), γ-aminobutyric acid (GABA), lactate (Lac), alanine (Ala).

and glutamine and distinct C4, C3 and C2 time courses of GABA, as well as C3 resonance of lactate and alanine as well as aspartate C2 [28]. C3 and C2 positions of glutamate and glutamine appeared overlapped, which limited the choice of the modelling strategy to a single compartment to avoid fixing *a priori* flux values in a two-compartment modelling approach. An MRS-derived input function could be included in the model with the accessibility of the ^{13}C lactate FE during the experiment, whereas in previous studies with direct detection the input function had to be imposed as *a priori* knowledge derived from standardized infusion protocols [29]. Indeed, most NMR sequences for indirect detection are able to quantify the concentration of ^{13}C and ^{12}C simultaneously allowing a direct measurement of the FE without the requirement of assumptions on the pool size over the experiment, as previously demonstrated [51]. Successful results in the detection of glutamate, glutamine and GABA resonances were similarly obtained in a volume of 16.5 μL in the dorsal hippocampus [31] and of barely 8.7 μL in the hypothalamic region [30]: time courses of glutamate and glutamine C4 were detected separately as well as GABA at the positions C2, C3 and C4. This constitutes a noticeable challenge since coil detection power diminishes with distance from the volume of interest, which greatly increases in the hypothalamus, located at the bottom of the brain. Metabolic modelling of the aforementioned results using a one-compartment model for brain metabolism assessed averaged TCA cycle (V_{TCA}), transmitochondrial flux (V_x), neurotransmission rate (V_{NT}) and pyruvate dilution flux (K_{dil}) [28,30]. Although these results constituted a novelty in the field of ^{13}C *in vivo* detection in the mouse brain, given the exceptionally small size of the volume of interest, two-compartmental modelling of glucose metabolism remains a prerogative of experiments performed with direct detection techniques in which glutamate and glutamine resonances appear fully separated [27,29], leading to additional estimation of TCA cycle rate in neurons (V_{TCA}^{n}) and astrocytes (V_g) and pyruvate carboxylase activity (V_{PC}). On the whole, these outcomes suggest an increased detection power in ^{13}C detection *in vivo* that leads toward quantification of region-specific metabolic fluxes in the mouse brain.

5. Conclusion

In the recent years, *in vivo* brain ^{13}C MRS has reached a level of relative maturity in animal experimentation, although the technique remains intrinsically challenging and requires high level instrumentations and complex knowledge. In conclusion, present standards make the detection of highly detailed metabolic information in the mouse brain possible without drawing upon cryogenic cooling of the coils or hyperpolarized substrates. Spectral quality reaches nowadays similar standards as in rat experiments, despite the reduced voxel size, thanks to the utilization of ultrahigh fields (Fig. 4). Specific insights on regional metabolism in the mouse brain and specific roles of GABAergic and glutamatergic neuronal metabolism need to be further investigated remaining so far confined to *ex vivo* investigations. The use of *in vivo* brain ^{13}C MRS in mice specific models of brain diseases is another promising application.

Acknowledgements

This work was supported by Centre d'Imagerie BioMédicale (CIBM) of the UNIL, UNIGE, HUG, CHUV, EPFL, and the Leenaards and Jeantet Foundations, Grant FP7-PEOPLE-2010-ITN-264780 and Swiss National Science Foundation Grant n.31003A_149983. The authors thank Dr Eulalia Serés Roig for her help in revising the content on RF coil designs and in providing interesting references in the field.

References

[1] N. Beckmann, J. Seelig, H. Wick, Analysis of glycogen storage disease by in vivo 13C NMR: comparison of normal volunteers with a patient, Magn. Reson Med. 16 (1990) 150–160.
[2] R. Gruetter, D.L. Rothman, E.J. Novotny, R.G. Shulman, Localized 13C NMR spectroscopy of myo-inositol in the human brain in vivo, Magn. Reson Med. 25 (1992) 204–210.
[3] D.L. Rothman, E.J. Novotny, G.I. Shulman, A.M. Howseman, O.A. Petroff, G. Mason, et al., 1H-[13C] NMR measurements of [4-13C]glutamate turnover in human brain, Proc. Natl. Acad. Sci. U. S. A. 89 (1992) 9603–9606.
[4] R. Gruetter, E.J. Novotny, S.D. Boulware, G.F. Mason, D.L. Rothman, G.I. Shulman, et al., Localized 13C NMR spectroscopy in the human brain of amino acid labeling from d-[1-13C]Glucose, J. Neurochem. 63 (1994) 1377–1385, http://dx.doi.org/10.1046/j.1471-4159.1994.63041377.x.
[5] R. Gruetter, G. Adriany, H. Merkle, P.M. Andersen, Broadband decoupled, 1H-localized 13C MRS of the human brain at 4 tesla, Magnetic Reson. Med. 36 (1996) 659–664, http://dx.doi.org/10.1002/mrm.1910360503.
[6] S. Blüml, In VivoQuantitation of cerebral metabolite concentrations using natural abundance13C MRS at 1.5 T, J. Magnetic Reson. 136 (1999) 219–225, http://dx.doi.org/10.1006/jmre.1998.1618.
[7] K.L. Behar, O. a. C. Petroff, J.W. Prichard, J.R. Alger, R.G. Shulman, Detection of metabolites in rabbit brain by 13C NMR spectroscopy following administration of [1-13C]glucose, Magn. Reson Med. 3 (1986) 911–920, http://dx.doi.org/10.1002/mrm.1910030611.
[8] W. Chen, G. Adriany, X.-H. Zhu, R. Gruetter, K. Ugurbil, Detecting natural abundance carbon signal of NAA metabolite within 12-cm3 localized volume of human brain using 1H-{13C} NMR spectroscopy, Magn. Reson. Med. 40 (1998) 180–184, http://dx.doi.org/10.1002/mrm.1910400203.
[9] C.R. Malloy, A.D. Sherry, F.M. Jeffrey, Carbon flux through citric acid cycle pathways in perfused heart by 13C NMR spectroscopy, FEBS Lett. 212 (1987) 58–62.
[10] C.R. Malloy, A.D. Sherry, F.M. Jeffrey, Evaluation of carbon flux and substrate selection through alternate pathways involving the citric acid cycle of the heart by 13C NMR spectroscopy, J. Biol. Chem. 263 (1988) 6964–6971.
[11] E.M. Chance, S.H. Seeholzer, K. Kobayashi, J.R. Williamson, Mathematical analysis of isotope labeling in the citric acid cycle with applications to 13C NMR studies in perfused rat hearts, J. Biol. Chem. 258 (1983) 13785–13794.
[12] W. Wiechert, 13C metabolic flux analysis, Metab. Eng. 3 (2001) 195–206, http://dx.doi.org/10.1006/mben.2001.0187.
[13] P.-G. Henry, G. Öz, S. Provencher, R. Gruetter, Toward dynamic isotopomer analysis in the rat brain in vivo: automatic quantitation of 13C NMR spectra using LCModel, NMR Biomed. 16 (2003) 400–412, http://dx.doi.org/10.1002/nbm.840.
[14] A. Shestov, J. Valette, D. Deelchand, K. Uğurbil, P.-G. Henry, Metabolic modeling of dynamic brain 13C NMR multiplet data: concepts and simulations with a two-compartment neuronal-glial model, Neurochem. Res. (2012) 1–14, http://dx.doi.org/10.1007/s11064-012-0782-5.
[15] M. Dehghani, M.,B. Lanz, J.M.N. Duarte, N. Kunz, R. Gruetter, Refined analysis of brain energy metabolism using in vivo dynamic enrichment of 13C multiplets, ASN Neuro 8 (2016), http://dx.doi.org/10.1177/1759091416632342.
[16] B. Tiret, A.A. Shestov, J. Valette, P.-G. Henry, Metabolic modeling of dynamic 13C NMR isotopomer data in the brain in vivo: fast screening of metabolic models using automated generation of differential equations, Neurochem. Res. 40 (2015) 2482–2492, http://dx.doi.org/10.1007/s11064-015-1748-1.
[17] G. Öz, I. Tkáč, K. Uğurbil, Animal models and high field imaging and spectroscopy, Dialogues Clin. Neurosci. 15 (2013) 263–278.
[18] N.R. Sibson, A. Dhankhar, G.F. Mason, K.L. Behar, D.L. Rothman, R.G. Shulman, In vivo 13C NMR measurements of cerebral glutamine synthesis as evidence for glutamate–glutamine cycling, Pnas 94 (1997) 2699–2704.
[19] N.R. Sibson, G.F. Mason, J. Shen, G.W. Cline, A.Z. Herskovits, J.E.M. Wall, et al., In vivo13C NMR measurement of neurotransmitter glutamate cycling, anaplerosis and TCA cycle flux in rat brain during [2-13C]glucose infusion, J. Neurochem. 76 (2001) 975–989, http://dx.doi.org/10.1046/j.1471-4159.2001.00074.x.
[20] R.A. de Graaf, G.F. Mason, A.B. Patel, D.L. Rothman, K.L. Behar, Regional glucose metabolism and glutamatergic neurotransmission in rat brain in vivo, Pnas 101 (2004) 12700–12705, http://dx.doi.org/10.1073/pnas.0405065101.
[21] P. van Eijsden, K.L. Behar, G.F. Mason, K.P.J. Braun, R.A. de Graaf, In vivo neurochemical profiling of rat brain by 1H-[13C] NMR spectroscopy. cerebral energetics and glutamatergic/GABAergic neurotransmission, J. Neurochem. 112 (2010) 24–33, http://dx.doi.org/10.1111/j.1471-4159.2009.06428.x.
[22] J.M.N. Duarte, B. Lanz, R. Gruetter, Compartmentalized cerebral metabolism of [1,6–13C]glucose determined by in vivo 13C NMR spectroscopy at 14.1 T, Front. Neuroenergetics 3 (2011), http://dx.doi.org/10.3389/fnene.2011.00003.
[23] J.M.N. Duarte, R. Gruetter, Glutamatergic and GABAergic energy metabolism measured in the rat brain by 13C NMR spectroscopy at 14.1 T, J. Neurochem. 126 (2013) 579–590, http://dx.doi.org/10.1111/jnc.12333.
[24] B. Lanz, L. Xin, P. Millet, R. Gruetter, In vivo quantification of neuro-glial metabolism and glial glutamate concentration using 1H-[13C] MRS at 14.1T, J. Neurochem. 128 (2014) 125–139, http://dx.doi.org/10.1111/jnc.12479.

[25] J.M.N. Duarte, F.-M. Girault, R. Gruetter, Brain energy metabolism measured by 13C magnetic resonance spectroscopy in vivo upon infusion of [3-13C] lactate, J. Neurosci. Res. 93 (2015) 1009–1018, http://dx.doi.org/10.1002/jnr.23531.
[26] G.F. Mason, D.L. Rothman, Basic principles of metabolic modeling of NMR 13C isotopic turnover to determine rates of brain metabolism in vivo, Metab. Eng. 6 (2004) 75–84, http://dx.doi.org/10.1016/j.ymben.2003.10.003.
[27] C.i.h.c. Nabuurs, D.w.j. Klomp, A. Veltien, H.e. Kan, A. Heerschap, Localized sensitivity enhanced in vivo 13C MRS to detect glucose metabolism in the mouse brain, Magnetic Reson. Med. 59 (2008) 626–630, http://dx.doi.org/10.1002/mrm.21498.
[28] L. Xin, B. Lanz, H. Lei, R. Gruetter, Assessment of metabolic fluxes in the mouse brain in vivo using 1H-[13C] NMR spectroscopy at 14.1 Tesla, J. Cereb. Blood Flow. Metab. 35 (2015) 759–765, http://dx.doi.org/10.1038/jcbfm.2014.251.
[29] M. Lai, B. Lanz, C.J. del C. Romero, C.R. Cudalbu, R. Gruetter, In vivo 13C MRS in the mouse brain at 14.1 T and metabolic flux quantification during infusion of [1,6–13C2] Glucose. In Proceedings of the Joint Annual Meeting ISMRM-ESMRMB, Milan, Italy. p.535, (2014).
[30] B. Lizarbe, A. Cherix, L. Xin, H. Lei, R. Gruetter, In vivo detection of hypothalamic glucose metabolism in HFD and regular fed mice. In Proceedings of the 24th Annual Meeting ISMRM, Singapore. p.110, (2016).
[31] A. Cherix, B. Lizarbe, H. Lei, R. Gruetter, In vivo measurement of metabolic fluxes in mouse dorsal hippocampus using 1H-[13C] NMR spectroscopy at 14.1 Tesla. In Proceedings of the 24th Annual Meeting ISMRM, Singapore. p.3969, (2016).
[32] F.C. Courtice, The blood volume of normal animals, J. Physiol. 102 (1943) 290–305.
[33] G. Dreyer, W. Ray, The blood volume of mammals as determined by experiments upon rabbits, Guinea-Pigs, and mice; and its relationship to the body weight and to the surface area expressed in a formula, Philosophical transactions. r. soc. Lond. B Biol. Sci. 201 (1911) 133–160, http://dx.doi.org/10.1098/rstb.1911.0003.
[34] H.B. Lee, M.D. Blaufox, Blood volume in the rat, J. Nucl. Med. 26 (1985) 72–76.
[35] National Center for the Remplacement, Refinement & Reduction of Animals in Research, UK. Decision Tree for Blood Sampling in Mice, 2016. https://www.nc3rs.org.uk/mouse-decision-tree-blood-sampling (accessed May 09, 2016).
[36] National Center for the Remplacement, Refinement & Reduction of Animals in Research, UK., Decision Tree for Blood Sampling in Rats, 2016. https://www.nc3rs.org.uk/rat-decision-tree-blood-sampling (accessed May 09, 2016).
[37] S. Parasuraman, R. Raveendran, R. Kesavan, Blood sample collection in small laboratory animals, J. Pharmacol. Pharmacother. 1 (2010) 87–93, http://dx.doi.org/10.4103/0976-500X.72350.
[38] M.W. McGuill, A.N. Rowan, Biological effects of blood loss: implications for sampling volumes and techniques, Ilar J. 31 (1989) 5–20, http://dx.doi.org/10.1093/ilar.31.4.5.
[39] J.J. Skillman, J. Hedley-Whyte, J.A. Pallotta, Cardiorespiratory, metabolic and endocrine changes after hemorrhage in man, Ann. Surg. 174 (1971) 911–922.
[40] A. D'Alessandro, H.B. Moore, E.E. Moore, M. Wither, T. Nemkov, E. Gonzalez, et al., Early hemorrhage triggers metabolic responses that build up during prolonged shock, Am J. Physio. Regulatory, Integr. Comp. Physio. 308 (2015) R1034–R1044, http://dx.doi.org/10.1152/ajpregu.00030.2015.
[41] M. Sack, F. Wetterling, A. Sartorius, G. Ende, W. Weber-Fahr, Signal-to-noise ratio of a mouse brain 13C CryoProbeTM system in comparison with room temperature coils: spectroscopic phantom and in vivo results, NMR Biomed. 27 (2014) 709–715, http://dx.doi.org/10.1002/nbm.3110.
[42] P.-G. Henry, D.K. Deelchand, I. Iltis, M. Marjanska, G. Öz, A.A. Shestov, et al., In Vivo 13C magnetic resonance spectroscopy and metabolic modeling: methodology, in: I.-Y. Choi, R. Gruetter (Eds.), Neural Metabolism in Vivo, Springer, US, Boston, MA, 2012, pp. 181–220. http://link.springer.com/chapter/10.1007/978-1-4614-1788-0_7?null (accessed September 27, 2012).
[43] B. Lanz, R. Gruetter, J.M.N. Duarte, Metabolic flux and compartmentation analysis in the brain in vivo, Vivo 4 (2013) 156, http://dx.doi.org/10.3389/fendo.2013.00156.
[44] C. Crone, Facilitated transfer of glucose from blood into brain tissue, J. Physiol. 181 (1965) 103–113.
[45] L. Hertz, G.A. Dienel, Lactate transport and transporters: general principles and functional roles in brain cells, J. Neurosci. Res. 79 (2005) 11–18, http://dx.doi.org/10.1002/jnr.20294.
[46] D.K. Deelchand, A.A. Shestov, D.M. Koski, K. Uğurbil, P.-G. Henry, Acetate transport and utilization in the rat brain, J. Neurochem. 109 (2009) 46–54, http://dx.doi.org/10.1111/j.1471-4159.2009.05895.x.
[47] B.M. Jucker, T.R. Schaeffer, R.E. Haimbach, T.S. McIntosh, D. Chun, M. Mayer, et al., Normalization of skeletal muscle glycogen synthesis and glycolysis in rosiglitazone-treated Zucker fatty rats, Diabetes 51 (2002) 2066–2073, http://dx.doi.org/10.2337/diabetes.51.7.2066.
[48] P.-G. Henry, G. Adriany, D. Deelchand, R. Gruetter, M. Marjanska, G. Öz, et al., In vivo 13C NMR spectroscopy and metabolic modeling in the brain: a practical perspective, Magn. Reson. Imaging 24 (2006) 527–539, http://dx.doi.org/10.1016/j.mri.2006.01.003.
[49] R.A. de Graaf, Basic Principles, in: in Vivo NMR Spectroscopy, John Wiley & Sons, Ltd, 2007, pp. 1–42. http://onlinelibrary.wiley.com/doi/10.1002/9780470512968.ch1/summary (accessed May 10, 2016).
[50] P.-G. Henry, I. Tkáč, R. Gruetter, 1H-localized broadband 13C NMR spectroscopy of the rat brain in vivo at 9.4 T, Magnetic Reson. Med. 50 (2003) 684–692, http://dx.doi.org/10.1002/mrm.10601.
[51] L. Xin, V. Mlynárik, B. Lanz, H. Frenkel, R. Gruetter, 1H-[13C] NMR spectroscopy of the rat brain during infusion of [2-13C] acetate at 14.1 T, Magnetic Reson. Med. 64 (2010) 334–340, http://dx.doi.org/10.1002/mrm.22359.
[52] D.I. Hoult, R.E. Richards, The signal-to-noise ratio of the nuclear magnetic resonance experiment, J. Magnetic Reson. 24 (1976) (1969) 71–85, http://dx.doi.org/10.1016/0022-2364(76)90233-X.
[53] T.W. Redpath, Signal-to-noise ratio in MRI, BJR 71 (1998) 704–707, http://dx.doi.org/10.1259/bjr.71.847.9771379.
[54] D.I. Hoult, P.C. Lauterbur, The sensitivity of the zeugmatographic experiment involving human samples, J. Magnetic Reson. 34 (1979) (1969) 425–433, http://dx.doi.org/10.1016/0022-2364(79)90019-2.
[55] P.A. Valdes Hernandez, A. Sumiyoshi, H. Nonaka, R. Haga, E. Aubert Vasquez, T. Ogawa, et al., An in vivo MRI template set for morphometry, tissue segmentation, and fMRI localization in rats, Vivo 5 (2011) 26, http://dx.doi.org/10.3389/fninf.2011.00026.
[56] N. Kovačević, J.T. Henderson, E. Chan, N. Lifshitz, J. Bishop, A.C. Evans, et al., A three-dimensional MRI atlas of the mouse brain with estimates of the average and variability, Cereb. Cortex 15 (2005) 639–645, http://dx.doi.org/10.1093/cercor/bhh165.
[57] R. Gruetter, C. Boesch, Fast, noniterative shimming of spatially localized signals. in vivo analysis of the magnetic field along axes, J. Magnetic Reson. 96 (1992) (1969) 323–334, http://dx.doi.org/10.1016/0022-2364(92)90085-L.
[58] R. Gruetter, Automatic, localized in vivo adjustment of all first-and second-order shim coils, Magnetic Reson. Med. 29 (1993) 804–811, http://dx.doi.org/10.1002/mrm.1910290613.
[59] M.H. Levitt, Spin Dynamics: Basics of Nuclear Magnetic Resonance, Wiley, 2001.
[60] L.O. Sillerud, J.R. Alger, R.G. Shulman, High-resolution proton NMR studies of intracellular metabolites in yeast using 13C decoupling, J. Magnetic Reson. 45 (1981) (1969) 142–150, http://dx.doi.org/10.1016/0022-2364(81)90108-6.
[61] T. Ogino, Y. Arata, S. Fujiwara, Proton correlation nuclear magnetic resonance study of metabolic regulations and pyruvate transport in anaerobic Escherichia coli cells, Biochemistry 19 (1980) 3684–3691.
[62] D. Foxall, J. Cohen, R. Tschudin, Selective observation of 13C-enriched metabolites by 1H NMR, J. Magnetic Reson. 51 (1983) (1969) 330–334, http://dx.doi.org/10.1016/0022-2364(83)90019-7.
[63] K.M. Brindle, J. Boyd, I.D. Campbell, R. Porteous, N. Soffe, Observation of carbon labelling in cell metabolites using proton spin echo NMR, Biochem. Biophys. Res. Commun. 109 (1982) 864–871.
[64] D.L. Rothman, K.L. Behar, H.P. Hetherington, J.A. den Hollander, M.R. Bendall, O.A. Petroff, et al., 1H-Observe/13C-decouple spectroscopic measurements of lactate and glutamate in the rat brain in vivo, Proc. Natl. Acad. Sci. U. S. A. 82 (1985) 1633–1637.
[65] S.M. Fitzpatrick, H.P. Hetherington, K.L. Behar, R.G. Shulman, The flux from glucose to glutamate in the rat brain in vivo as determined by 1H-observed, 13C-edited NMR spectroscopy, J. Cereb. Blood Flow. Metab. 10 (1990) 170–179, http://dx.doi.org/10.1038/jcbfm.1990.32.
[66] R. Gruetter, G. Adriany, I.-Y. Choi, P.-G. Henry, H. Lei, G. Öz, Localized in vivo13C NMR spectroscopy of the brain, NMR Biomed. 16 (2003) 313–338, http://dx.doi.org/10.1002/nbm.841.
[67] N. Beckmann, Carbon-13 NMR Spectroscopy of Biological Systems, Academic Press, 1995.
[68] S. Cerdan, B. Künnecke, J. Seelig, Cerebral metabolism of [1,2-13C2]acetate as detected by in vivo and in vitro 13C NMR, J. Biol. Chem. 265 (1990) 12916–12926.
[69] N. Beckmann, S. Müller, Natural-abundance 13C spectroscopic imaging applied to humans, J. Magnetic Reson. 93 (1991) (1969) 186–194, http://dx.doi.org/10.1016/0022-2364(91)90041-Q.
[70] N. Beckmann, I. Turkalj, J. Seelig, U. Keller, 13C NMR for the assessment of human brain glucose metabolism in vivo, Biochemistry 30 (1991) 6362–6366.
[71] R. Gruetter, E.J. Novotny, S.D. Boulware, D.L. Rothman, G.F. Mason, G.I. Shulman, et al., Direct measurement of brain glucose concentrations in humans by 13C NMR spectroscopy, Proc. Natl. Acad. Sci. U. S. A. 89 (1992) 1109–1112.
[72] P.B. Barker, X. Golay, D. Artemov, R. Ouwerkerk, M.A. Smith, A. j. Shaka, Broadband proton decoupling for in vivo brain spectroscopy in humans, Magn. Reson. Med. 45 (2001) 226–232, http://dx.doi.org/10.1002/1522-2594(200102)45:2<226::AID-MRM1031>3.0.CO;2-Z.
[73] D. w. j. Klomp, W. k. j. Renema, M. van der Graaf, B. e. de Galan, A. p. m. Kentgens, A. Heerschap, Sensitivity-enhanced 13C MR spectroscopy of the human brain at 3 Tesla, Magn. Reson. Med. 55 (2006) 271–278, http://dx.doi.org/10.1002/mrm.20745.
[74] D.W.J. Klomp, A.P.M. Kentgens, A. Heerschap, Polarization transfer for sensitivity-enhanced MRS using a single radio frequency transmit channel, NMR Biomed. 21 (2008) 444–452, http://dx.doi.org/10.1002/nbm.1208.
[75] B. Tiffon, J. Mispelter, J.-M. Lhoste, A carbon-13 in Vivo double surface-coil NMR probe with efficient low-power proton decoupling at 400 MHz using

the WALTZ-16 sequence, J. Magnetic Reson. 68 (1986) (1969) 544–550, http://dx.doi.org/10.1016/0022-2364(86)90344-6.
[76] J. Mispelter, B. Tiffon, E. Quiniou, J.M. Lhoste, Optimization of 13C-{1H} double coplanar surface-coil design for the WALTZ-16 decoupling sequence, J. Magnetic Reson. 82 (1989) (1969) 622–628, http://dx.doi.org/10.1016/0022-2364(89)90226-6.
[77] N.V. Reo, C.S. Ewy, B.A. Siegfried, J.J.H. Ackerman, High-field 13C NMR spectroscopy of tissue in vivo. a double-resonance surface-coil probe, J. Magnetic Reson. 58 (1984) 76–84, http://dx.doi.org/10.1016/0022-2364(84)90008-8.
[78] T.M. Grist, A. Jesmanowicz, J.B. Kneeland, W. Froncisz, J.S. Hyde, Doubly tuned local coils for MRI and MRS at 1.5 T, Magn. Reson. Med. 6 (1988) 253–264, http://dx.doi.org/10.1002/mrm.1910060303.
[79] J.A. den Hollander, K.L. Behar, R.G. Shulman, Use of double-tuned surface coils for the application of 13C NMR to brain metabolism, J. Magnetic Reson. 57 (1984) (1969) 311–313, http://dx.doi.org/10.1016/0022-2364(84)90132-X.
[80] R.A. de Graaf, Radiofrequency pulses, in: In Vivo NMR Spectroscopy, John Wiley & Sons, Ltd, 2007, pp. 233–295. http://onlinelibrary.wiley.com/doi/10.1002/9780470512968.ch5/summary (accessed September 26, 2016).
[81] S. Li, Y. Zhang, S. Wang, M.F. Araneta, C.S. Johnson, Y. Xiang, et al., 13C MRS of occipital and frontal lobes at 3 T using a volume coil for stochastic proton decoupling, NMR Biomed. 23 (2010) 977–985, http://dx.doi.org/10.1002/nbm.1524.
[82] P.A. Bottomley, P.B. Roemer, Homogeneous tissue model estimates of RF power deposition in human NMR studies: local elevations predicted in surface coil decoupling, Ann. N. Y. Acad. Sci. 649 (1992) 144–159.
[83] J.R. Keltner, J.W. Carlson, M.S. Roos, S.T.S. Wong, T.L. Wong, T.F. Budinger, Electromagnetic fields of surface coil in vivo NMR at high frequencies, Magnetic Reson. Med. 22 (1991) 467–480.
[84] G. Adriany, R. Gruetter, A half-volume coil for efficient proton decoupling in humans at 4 tesla, J. Magnetic Reson. 125 (1997) 178–184, http://dx.doi.org/10.1006/jmre.1997.1113.
[85] F.D. Doty, G. Entzminger, J. Kulkarni, K. Pamarthy, J.P. Staab, Radio frequency coil technology for small-animal MRI, NMR Biomed. 20 (2007) 304–325, http://dx.doi.org/10.1002/nbm.1149.
[86] M. Garwood, K. Uğurbil, B 1 insensitive adiabatic RF pulses, in: P.M. Rudin (Ed.), In-vivo Magnetic Resonance Spectroscopy I: Probeheads and Radio-frequency Pulses Spectrum Analysis, Springer, Berlin Heidelberg, 1992, pp. 109–147. http://link.springer.com/chapter/10.1007/978-3-642-45697-8_4 (accessed September 27, 2016).
[87] K. Uğurbil, M. Garwood, A.R. Rath, M. Robin Bendall, Amplitude- and frequency/phase-modulated refocusing pulses that induce plane rotations even in the presence of inhomogeneous B1 fields, J. Magnetic Reson. 78 (1988) (1969) 472–497, http://dx.doi.org/10.1016/0022-2364(88)90133-3.
[88] M. Garwood, Y. Ke, Symmetric pulses to induce arbitrary flip angles with compensation for rf inhomogeneity and resonance offsets, J. Magnetic Reson. 94 (1991) 511–525, http://dx.doi.org/10.1016/0022-2364(91)90137-I.
[89] A. Haase, F. Odoj, M. Von Kienlin, J. Warnking, F. Fidler, A. Weisser, et al., NMR probeheads for in vivo applications, Concepts Magn. Reson 12 (2000) 361–388, http://dx.doi.org/10.1002/1099-0534(2000)12:6<361::AID-CMR1>3.0.CO;2-L.
[90] R.A. de Graaf, Hardware, in: in Vivo NMR Spectroscopy, John Wiley & Sons, Ltd, 2007, pp. 479–548. http://onlinelibrary.wiley.com/doi/10.1002/9780470512968.ch10/summary (accessed June 14, 2016).
[91] D.H. Anderson, Compartmental Modeling and Tracer Kinetics, Springer Berlin Heidelberg, Berlin, Heidelberg, 1983. http://link.springer.com/10.1007/978-3-642-51861-4 (accessed September 04, 2015).
[92] J.A. Jacquez, Compartmental Analysis in Biology and Medicine, Second Edition, second ed., University of Michigan Press, Ann Arbor, 1985.
[93] J.M.N. Duarte, R. Gruetter, Glutamatergic and GABAergic energy metabolism measured in the rat brain by 13C NMR spectroscopy at 14.1 T, J. Neurochem. 126 (2013) 579–590, http://dx.doi.org/10.1111/jnc.12333.
[94] D. Manor, D.L. Rothman, G.F. Mason, F. Hyder, O. a. C. Petroff, K.L. Behar, The rate of turnover of cortical GABA from [1-13C]glucose is reduced in rats treated with the GABA-transaminase inhibitor vigabatrin (γ-vinyl GABA), Neurochem. Res. 21 (1996) 1031–1041, http://dx.doi.org/10.1007/BF02532413.
[95] V. Tiwari, S. Ambadipudi, A.B. Patel, Glutamatergic and GABAergic TCA cycle and neurotransmitter cycling fluxes in different regions of mouse brain, J. Cereb. Blood Flow Metabolism 33 (2013) 1523–1531, http://dx.doi.org/10.1038/jcbfm.2013.114.
[96] G.M. Chowdhury, A.B. Patel, G.F. Mason, D.L. Rothman, K.L. Behar, Glutamatergic and GABAergic neurotransmitter cycling and energy metabolism in rat cerebral cortex during postnatal development, J. Cereb. Blood Flow. Metab. 27 (2007) 1895–1907, http://dx.doi.org/10.1038/sj.jcbfm.9600490.
[97] J. Jacquez, C. Simon, Qualitative theory of compartmental systems, SIAM Rev. 35 (1993) 43–79, http://dx.doi.org/10.1137/1035003.
[98] Tracer Kinetics in Biomedical Research, Kluwer Academic Publishers, Boston, 2002. http://link.springer.com/10.1007/b112199 (accessed September 03, 2015).
[99] B. Lanz, L. Xin, P. Millet, R. Gruetter, In vivo quantification of neuro-glial metabolism and glial glutamate concentration using 1H-[13C] MRS at 14.1T, J. Neurochem. 128 (2014) 125–139, http://dx.doi.org/10.1111/jnc.12479.
[100] R. Gruetter, E.R. Seaquist, K. Ugurbil, A mathematical model of compartmentalized neurotransmitter metabolism in the human brain, Am. J. Physiol. Endocrinol. Metab. 281 (2001) E100–E112.
[101] A.B. Patel, R.A. de Graaf, G.F. Mason, D.L. Rothman, R.G. Shulman, K.L. Behar, The contribution of GABA to glutamate/glutamine cycling and energy metabolism in the rat cortex in vivo, Pnas 102 (2005) 5588–5593, http://dx.doi.org/10.1073/pnas.0501703102.
[102] I.-Y. Choi, H. Lei, R. Gruetter, Effect of deep pentobarbital anesthesia on neurotransmitter metabolism in vivo: on the correlation of total glucose consumption with glutamatergic action, J. Cereb. Blood Flow. Metab. 22 (2002) 1343–1351, http://dx.doi.org/10.1097/01.WCB.0000040945.89393.46.
[103] O.P. Ottersen, N. Zhang, F. Walberg, Metabolic compartmentation of glutamate and glutamine: morphological evidence obtained by quantitative immunocytochemistry in rat cerebellum, Neuroscience 46 (1992) 519–534, http://dx.doi.org/10.1016/0306-4522(92)90141-N.
[104] N. Zhang, J. Laake, E. Nagelhus, J. Storm-Mathisen, O.P. Ottersen, Distribution of glutamine-like immunoreactivity in the cerebellum of rat and baboon (Papio anubis) with reference to the issue of metabolic compartmentation, Anat. Embryol. 184 (1991) 213–223, http://dx.doi.org/10.1007/BF01673257.
[105] I. Tkác, P.-G. Henry, P. Andersen, C.D. Keene, W.C. Low, R. Gruetter, Highly resolved in vivo 1H NMR spectroscopy of the mouse brain at 9.4 T, Magn. Reson Med. 52 (2004) 478–484, http://dx.doi.org/10.1002/mrm.20184.
[106] I. Tkáč, R. Rao, M.K. Georgieff, R. Gruetter, Developmental and regional changes in the neurochemical profile of the rat brain determined by in vivo 1H NMR spectroscopy, Magn. Reson. Med. 50 (2003) 24–32, http://dx.doi.org/10.1002/mrm.10497.
[107] A.A. Shestov, J. Valette, K. Uğurbil, P.-G. Henry, On the reliability of 13C metabolic modeling with two-compartment neuronal-glial models, J. Neurosci. Res. 85 (2007) 3294–3303, http://dx.doi.org/10.1002/jnr.21269.
[108] M. Merle, J.-M. Franconi, Brain metabolic compartmentalization, metabolism modeling, and cerebral activity-metabolism relationship, in: I.-Y. Choi, R. Gruetter (Eds.), Neural Metabolism in Vivo, Springer, US, 2012, pp. 947–992. http://www.springerlink.com/content/r36g4u13w80181j6/abstract/ (accessed May 25, 2012).
[109] E. Carson, C. Cobelli, Modeling Methodology for Physiology and Medicine, Newnes, 2013.
[110] G.C. Canavos, A Monte Carlo Investigation of Experimental Data Requirements for Fitting Polynomial Functions, 1974. http://ntrs.nasa.gov/search.jsp?R=19740018957 (accessed September 27, 2016).
[111] H. Kuwabara, A.C. Evans, A. Gjedde, Michaelis-menten constraints improved cerebral glucose metabolism and regional lumped constant measurements with [18F]Fluorodeoxyglucose, J. Cereb. Blood Flow. Metab. 10 (1990) 180–189, http://dx.doi.org/10.1038/jcbfm.1990.33.
[112] Parameter Estimation, Some Fundamentals of Regression Analysis, in: Tracer Kinetics in Biomedical Research, Springer, US, 2002, pp. 215–281. http://link.springer.com/chapter/10.1007/0-306-46833-6_8 (accessed May 27, 2016).
[113] Parameter Estimation in Compartmental Models, in: Tracer Kinetics in Biomedical Research, Springer, US, 2002, pp. 307–335. http://link.springer.com/chapter/10.1007/0-306-46833-6_10 (accessed May 27, 2016).
[114] A.O. Nier, E.A. Gulbransen, Variations in the relative abundance of the carbon isotopes, J. Am. Chem. Soc. 61 (1939) 697–698, http://dx.doi.org/10.1021/ja01872a047.
[115] R.R. Ernst, W.A. Anderson, Application of fourier transform spectroscopy to magnetic resonance, Rev. Sci. Instrum. 37 (1966) 93–102, http://dx.doi.org/10.1063/1.1719961.
[116] P.C. Lauterbur, C13 nuclear magnetic resonance spectra, J. Chem. Phys. 26 (1957) 217–218, http://dx.doi.org/10.1063/1.1743253.
[117] E.D. Becker, T.C. Farrar, Fourier Transform Spectroscopy New methods dramatically improve the sensitivity of infrared and nuclear magnetic resonance spectroscopy, Science 178 (1972) 361–368, http://dx.doi.org/10.1126/science.178.4059.361.
[118] R.T. Eakin, L.O. Morgan, C.T. Gregg, N.A. Matwiyoff, Carbon-13 nuclear magnetic resonance spectroscopy of living cells and their metabolism of a specifically labeled 13C substrate, FEBS Lett. 28 (1972) 259–264, http://dx.doi.org/10.1016/0014-5793(72)80726-9.
[119] N.A. Matwiyoff, T.E. Needham, Carbon-13 nmr spectroscopy of red blood cell suspensions, Biochem. Biophysical Res. Commun. 49 (1972) 1158–1164, http://dx.doi.org/10.1016/0006-291X(72)90590-6.
[120] Alger, L.O. Sillerud, K.L. Behar, R.J. Gillies, R.G. Shulman, R.E. Gordon, et al., In vivo carbon-13 nuclear magnetic resonance studies of mammals, Science 214 (1981) 660–662, http://dx.doi.org/10.1126/science.7292005.
[121] H. Bachelard, Landmarks in the application of 13C-magnetic resonance spectroscopy to studies of neuronal/glial relationships, Dev. Neurosci. 20 (1998) 277–288.
[122] K. Ugurbil, T.R. Brown, J.A. den Hollander, P. Glynn, R.G. Shulman, High-resolution 13C nuclear magnetic resonance studies of glucose metabolism in Escherichia coli, Proc. Natl. Acad. Sci. U. S. A. 75 (1978) 3742–3746.
[123] J.A. den Hollander, T.R. Brown, K. Ugurbil, R.G. Shulman, 13C nuclear magnetic resonance studies of anaerobic glycolysis in suspensions of yeast cells, Proc. Natl. Acad. Sci. U. S. A. 76 (1979) 6096–6100.
[124] G.F. Mason, K.L. Behar, D.L. Rothman, R.G. Shulman, NMR determination of intracerebral glucose concentration and transport kinetics in rat brain, J. Cereb. Blood Flow. Metab. 12 (1992) 448–455, http://dx.doi.org/10.1038/jcbfm.1992.62.

[125] T.F. Vandamme, Use of rodents as models of human diseases, J. Pharm. Bioallied Sci. 6 (2014) 2–9, http://dx.doi.org/10.4103/0975-7406.124301.
[126] L. Sun, Animal models of glioma, in: A. Ghosh (Ed.), Glioma - Exploring its Biology and Practical Relevance, InTech, 2011. http://www.intechopen.com/books/glioma-exploring-its-biology-and-practical-relevance/animal-models-of-glioma (accessed June 26, 2012).
[127] N.R. Sibson, A. Dhankhar, G.F. Mason, D.L. Rothman, K.L. Behar, R.G. Shulman, Stoichiometric coupling of brain glucose metabolism and glutamatergic neuronal activity, Pnas 95 (1998) 316–321.
[128] J. Shen, R.E. Rycyna, D.L. Rothman, Improvements on an in vivo automatic shimming method (FASTERMAP), Magn. Reson. Med. 38 (1997) 834–839, http://dx.doi.org/10.1002/mrm.1910380521.
[129] J. Shen, K.F. Petersen, K.L. Behar, P. Brown, T.W. Nixon, G.F. Mason, et al., Determination of the rate of the glutamate/glutamine cycle in the human brain by in vivo 13C NMR, Pnas 96 (1999) 8235–8240, http://dx.doi.org/10.1073/pnas.96.14.8235.
[130] R. Gruetter, K. Ugurbil, E.R. Seaquist, Steady-state cerebral glucose concentrations and transport in the human brain, J. Neurochem. 70 (1998) 397–408, http://dx.doi.org/10.1046/j.1471-4159.1998.70010397.x.
[131] J. Pfeuffer, I. Tkáč, I.-Y. Choi, H. Merkle, K. Uğurbil, M. Garwood, et al., Localized in vivo 1H NMR detection of neurotransmitter labeling in rat brain during infusion of [1-13C] D-glucose, Magn. Reson. Med. 41 (1999) 1077–1083, http://dx.doi.org/10.1002/(SICI)1522-2594(199906)41:6<1077::AID-MRM1>3.0.CO;2-#.
[132] A.B. Patel, R.A. de Graaf, D.L. Rothman, K.L. Behar, G.F. Mason, Evaluation of cerebral acetate transport and metabolic rates in the rat brain in vivo using 1H-[13C]-NMR, J. Cereb. Blood Flow. Metab. 30 (2010) 1200–1213, http://dx.doi.org/10.1038/jcbfm.2010.2.
[133] G.F. Mason, D.L. Rothman, K.L. Behar, R.G. Shulman, NMR determination of the TCA cycle rate and alpha-ketoglutarate/glutamate exchange rate in rat brain, J. Cereb. Blood Flow. Metab. 12 (1992) 434–447, http://dx.doi.org/10.1038/jcbfm.1992.61.